The Functional Transcriptomic Landscape Informs Therapeutic Strategies in Multiple Myeloma

Praneeth Reddy Sudalagunta[1], Rafael R. Canevarolo[1], Mark B. Meads[2], Maria Silva[1], Xiaohong Zhao[2], Christopher L. Cubitt[3], Samer S. Sansil[3], Gabriel DeAvila[2], Raghunandan Reddy Alugubelli[2], Ryan T. Bishop[4], Alexandre Tungesvik[5], Qi Zhang[6], Oliver Hampton[6], Jamie K. Teer[7], Eric A. Welsh[7], Sean J. Yoder[8], Bijal D. Shah[2], Lori Hazlehurst[9], Robert A. Gatenby[10,11], Dane R. Van Domelen[12], Yi Chai[12], Feng Wang[12], Andrew DeCastro[12], Amanda M. Bloomer[13], Erin M. Siegel[13], Conor C. Lynch[4], Daniel M. Sullivan[2], Melissa Alsina[14], Taiga Nishihori[14], Jason Brayer[2], John L. Cleveland[4], William Dalton[15], Christopher J. Walker[12], Yosef Landesman[12], Rachid Baz[2], Ariosto S. Silva[1], and Kenneth H. Shain[2]

ABSTRACT

Several therapeutic agents have been approved for treating multiple myeloma, a cancer of bone marrow–resident plasma cells. Predictive biomarkers for drug response could help guide clinical strategies to optimize outcomes. In this study, we present an integrated functional genomic analysis of tumor samples from patients multiple myeloma that were assessed for their *ex vivo* drug sensitivity to 37 drugs, clinical variables, cytogenetics, mutational profiles, and transcriptomes. This analysis revealed a multiple myeloma transcriptomic topology that generates "footprints" in association with *ex vivo* drug sensitivity that have both predictive and mechanistic applications. Validation of the transcriptomic footprints for the anti-CD38 mAb daratumumab (DARA) and the nuclear export inhibitor selinexor (SELI) demonstrated that these footprints can accurately classify clinical responses. The analysis further revealed that DARA and SELI have anticorrelated mechanisms of resistance, and treatment with a SELI-based regimen immediately after a DARA-containing regimen was associated with improved survival in three independent clinical trials, supporting an evolutionary-based strategy involving sequential therapy. These findings suggest that this unique repository and computational framework can be leveraged to inform underlying biology and to identify therapeutic strategies to improve treatment of multiple myeloma.

Significance: Functional genomic analysis of primary multiple myeloma samples elucidated predictive biomarkers for drugs and molecular pathways mediating therapeutic response, which revealed a rationale for sequential therapy to maximize patient outcomes.

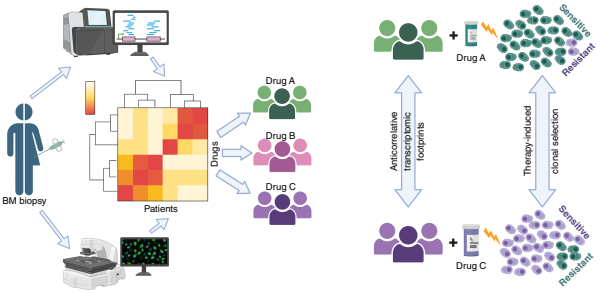

Introduction

Multiple myeloma remains an all but incurable cancer of bone marrow (BM)-resident plasma cells. Recent advances in multiple myeloma drug development have, however, led to significant improvements in patient outcomes (1), with the approval of immunomodulatory (IMID) agents, proteasome inhibitors (PI), mAbs, immunotherapies, and nuclear export inhibitors (2). Treatment of newly diagnosed patients with multiple myeloma consists of induction with a combination of agents, followed by high-dose chemotherapy and BM transplant in eligible patients, and

[1]Department of Metabolism and Physiology, Moffitt Cancer Center and Research Institute, Tampa, Florida. [2]Department of Malignant Hematology, Moffitt Cancer Center and Research Institute, Tampa, Florida. [3]Cancer Pharmacokinetics and Pharmacodynamics Core, Moffitt Cancer Center and Research Institute, Tampa, Florida. [4]Department of Tumor Microenvironment and Metastasis, Moffitt Cancer Center and Research Institute, Tampa, Florida. [5]Department of Internal Medicine, University of South Florida, Tampa, Florida. [6]Aster Insights (formerly M2Gen), Tampa, Florida. [7]Department of Biostatistics and Bioinformatics, Moffitt Cancer Center and Research Institute, Tampa, Florida. [8]Molecular Genomics Core, Moffitt Cancer Center and Research Institute, Tampa, Florida. [9]Department of Pharmaceutical Sciences, West Virginia University, Morgantown, West Virginia. [10]Department of Radiology, Moffitt Cancer Center and Research Institute, Tampa, Florida. [11]Department of Integrated Mathematical Oncology, Moffitt Cancer Center and Research Institute, Tampa, Florida. [12]Research and Translational Development, Karyopharm Therapeutics, Newton, Massachusetts. [13]Total Cancer Care, Moffitt Cancer Center, Tampa, Florida. [14]Department of Blood and Marrow Transplant and Cellular Therapies, Moffitt Cancer Center and Research Institute, Tampa, Florida. [15]Molecular Medicine Program, Moffitt Cancer Center and Research Institute, Tampa, Florida.

Corresponding Authors: Ariosto S. Silva, Moffitt Cancer Center Magnolia Campus, 12902 USF Magnolia Drive, Tampa, FL 33612. E-mail: Ariosto.Silva@moffitt.org; and Kenneth H. Shain, Ken.Shain@moffitt.org

Cancer Res 2025;85:378–98

doi: 10.1158/0008-5472.CAN-24-0886

maintenance therapy (3). Upon relapse, patients are treated with multiagent combinations, until the eventual emergence of refractory disease. Although diagnostic and prognostic biomarkers are fully integrated into characterization of multiple myeloma (4), there are no predictive biomarkers for clinical use, with choice of therapy upon relapse relying on clinical acumen (5).

Despite recent advances in next-generation sequencing technologies (6) to identify genomic and transcriptomic features (7), clinical molecular characterization of multiple myeloma disease still mostly relies on FISH cytogenetics and serum levels of soluble markers such as paraprotein, which do not account for the complex tumor heterogeneity (8). We propose that significant gains in clinical outcomes can be achieved by using next-generation sequencing–based predictive biomarkers that can simplify the complexity of the multiple choices of drug combinations a patient may receive and that can identify those that will lead to the best outcome (9, 10). In this study, we report the use of patient-specific *ex vivo* drug response from an established *ex vivo* drug screening tool [*Ex Vivo* Mathematical Myeloma Advisor (EMMA); refs. 9, 10] and paired molecular data to identify predictive biomarkers and inform critical multiple myeloma biology. Finally, we validate these biomarkers using paired molecular and clinical response data from an independent clinical trial and standard-of-care treatment.

EMMA is a label-free, nondestructive, high-throughput platform to characterize *ex vivo* drug sensitivity of primary multiple myeloma cells in a reconstruction of the myeloma microenvironment. In this system, BM aspirate–derived CD138-selected multiple myeloma cells are seeded in 384-well plates (which can be extended to 1,536-well plates) in coculture with BM stroma, the extracellular matrix, and patient-derived plasma and are tested with up to 31 drugs or combinations (127 drugs/combinations can be tested in a 1,536-well plate) simultaneously at five serially (1:3) diluted concentrations (including but not limited to the physiologically relevant range of concentrations for each drug, as determined from pharmacokinetic data from phase I clinical trials). In this platform, viability is assessed at 30-minute intervals through digital image analysis of label-free brightfield images over 6 days. The results from this high-dimensional assay (i.e., 288 time point measurements per well) parameterize patient-specific drug sensitivity mathematical models, which, when combined with drug-specific pharmacokinetic data, generate predictions of clinical outcome of single agents and combinations (9, 10). This *ex vivo* drug response database represents a unique resource to examine the biology of cells of patients with multiple myeloma in response to standard-of-care and preclinical therapeutics, including immunotherapies (9, 10).

To further examine the clinical utility of this platform, we have integrated *ex vivo* drug response with clinical cytogenetic abnormalities from FISH, bulk whole-exome sequencing (WES), and RNA sequencing (RNA-seq) data to derive genomic and transcriptomic traits that are associated with drug sensitivity in multiple myeloma (11, 12). We submit that this approach can inform multiple myeloma biology and personalized patient care. First, the *ex vivo* setting allows one to assess the response of patient $CD138^+$ malignant plasma cells to standard-of-care, trial experimental therapies, as well as preclinical drugs and combinations. Second, although clinically a patient with multiple myeloma can only receive one therapeutic regimen at a given point in time, primary samples can be simultaneously tested *ex vivo* with a large number of therapies. Finally, molecular characterization of *ex vivo* drug sensitivity can be assessed for each drug or combination individually as opposed to clinical response, which can only be associated with the entire combination.

Among the findings in this study, we confirmed previously identified predictive biomarkers in multiple myeloma, such as increased sensitivity of t(11;14)-harboring multiple myeloma cells to BCL2 inhibitor venetoclax (VEN; refs. 13, 14). Of special interest, we evaluate the predictive potential of *ex vivo*–derived transcriptomic footprints in patients treated with the CD38-directed mAb daratumumab (DARA) at Moffitt Cancer Center and the nuclear export inhibitor selinexor (SELI) in the BOSTON trial (NCT03110562; ref. 15). Furthermore, this functional genomic analysis identified drug pairs with anticorrelative transcriptomic footprints, suggesting that adaption to resistance to one drug would lead to increased sensitive to the other. As a proof of principle, we show that treating patients with multiple myeloma with a SELI-based regimen immediately after a DARA-containing regimen is associated with improved progression-free survival (PFS) in three independent clinical trials involving SELI, specifically BOSTON (NCT03110562; ref. 15), STOMP (NCT02343042; refs. 16, 17), and XPORT-MM-028 (NCT04414475; ref. 18). Collectively, these findings indicate that *ex vivo*–derived functional transcriptomic footprints can be used to inform multiple myeloma biology and to develop predictive biomarkers and novel therapeutic strategies for the treatment of patients with multiple myeloma.

Materials and Methods

Overview of the approach

We present a computational framework that maps the functional genomic landscape in multiple myeloma for a given drug by relying on RNA-seq, WES, and cytogenetic data of patients with multiple myeloma that are matched with *ex vivo* drug sensitivity measures of $CD138^+$ cells isolated from consented patients. An overview of the flow of information across various stages of this framework is depicted in **Fig. 1A**. The detailed methods for each step within the framework are provided in the subsequent sections. In brief, the workflow begins when a patient consents to the Total Cancer Care (TCC) protocol and donates BM specimen for research. The sorted $CD138^+$ cells are divided and characterized by performing WES, RNA-seq, and *ex vivo* drug sensitivity screening of several multiple myeloma drugs. Furthermore, the same patient's clinical data are abstracted to transcribe their treatment history and FISH data into a well-annotated database that can be used to programmatically query this information.

The cytogenetic abnormalities and mutated genes of patients identified from FISH and WES, respectively, characterize a patient's tumor genetically (presence or absence of a genetic event). RNA-seq data alone characterize the transcriptome of a patient's tumor, leading to a multiple myeloma–specific transcriptomic landscape. Finally, the *ex vivo* drug sensitivity metric, the area under the dose–response curve), characterizes a patient's *ex vivo* drug sensitivity to each drug tested. Using this approach, one can identify all functional (associated with a phenotype) genetic events that lead to sensitivity or resistance to a given drug across the entire multiple myeloma cohort, resulting in genetic biomarkers that can putatively predict *ex vivo* drug sensitivity in multiple myeloma. We then rely on paired RNA-seq and *ex vivo* drug sensitivity data from patient samples to infer transcriptomic footprints or biomarkers for resistance or sensitivity to each drug. These inferred biomarkers

are examined to develop novel therapeutic strategies in multiple myeloma.

Patient cohorts and primary cancer cells: Moffitt cohort

Patients were consented to the TCC protocol, the Moffitt Cancer Center's institutional biorepository (MCC#14690; Advarra Institutional Review Board Pro00014441). Patients agreed to donate additional BM aspirate during a clinical BM biopsy procedure, donated blood samples, and granted access to their medical records. Overall, a total of 1,136 BM specimens were collected from 892 patients with multiple myeloma, who signed informed consent to the TCC protocol (MCC#14690) at Moffitt Cancer Center (Moffitt TCC cohort). All primary multiple myeloma samples collected under the TCC protocol (MCC#14960) between October 19, 2011 and February 1, 2023 were considered for the study, which served as the only inclusion criterion, and no exclusion criteria were used. Of the 1,136 TCC samples, a total of 415 samples with more than 2 million $CD138^+$ cells were used for *ex vivo* drug sensitivity characterization. A subset of TCC multiple myeloma samples that yielded at least 1 million $CD138^+$ cells was considered for the Oncology Research Information Exchange Network (ORIEN) AVATAR program, which includes research use of only grade WES (900), RNA-seq (891), and germline sequencing data and a collection of deep longitudinal clinical data with lifetime follow-up. Apart from availability of sufficient $CD138^+$ cells and barring technical issues, there were no criteria that led to attrition of samples. Demographic information for the cohort can be found in Supplementary Table S1. Briefly, of the 892 patients with multiple myeloma, 490 patients had their biological sex identified as male and 402 as female, resulting in a 55/45 male-to-female biological sex ratio. Patients' weight was not collected as a variable in this study. Analysis of racial and ethnicity characteristics of the participants revealed that most of them were White (85%) and non-Hispanic (88%). The median age of the study participants at the time of sample collection was found to be 65 (30–94) years. Investigators obtained signed informed consent from all patients who were enrolled in the clinical trials/protocols MCC17814, MCC14745, MCC14690, and MCC18608 conducted at the H. Lee Moffitt Cancer Center and Research Institute, as approved by the Institutional Review Board. To this end, patient samples were used in accordance with the Declaration of Helsinki, International Ethical Guidelines for Biomedical Research Involving Human Subjects (Council for International Organizations of Medical Science), the Belmont Report, and the U.S. Common Rule. The medical records were de-identified in accordance with the TCC protocol, and only the following clinically relevant information was reviewed: (i) the treatment administered (therapeutic agents, doses, and schedule) prior to biopsy, (ii) cytogenetics, (iii) disease statuses, (iv) demographics, and (v) treatment outcomes. All other patient and sample characteristics were blinded

Data repository of patients with multiple myeloma: Moffitt cohort

At Moffitt Cancer Center, we have collected more than 1,136 samples of patients with multiple myeloma in total, and the tumor cells have been characterized for *ex vivo* drug sensitivity, molecular features, and clinical traits in partnership with the ORIEN/AVATAR consortium. **Figure 1B** presents a Circos plot featuring 415 samples screened for *ex vivo* drug sensitivity, 260 samples with WES, 891 samples with RNA-seq, and 146 samples with cytogenetic data abstracted. A total of 716 samples have WES data, RNA-seq data, and cytogenetic data; 199 of them also have *ex vivo* drug sensitivity data.

Supplementary Figure S1 presents an oncoplot for patients who have *ex vivo* drug sensitivity, RNA-seq, and WES data (239 patients), the top 10 most common mutations by frequency as rows and patients as columns, which are ordered by their disease states from smoldering multiple myeloma, newly diagnosed multiple myeloma, early relapsed/refractory multiple myeloma, to late relapsed/refractory multiple myeloma. The patients' cytogenetic abnormalities are also highlighted.

Ex vivo drug sensitivity characterization: Moffitt cohort

An *ex vivo* assay was used to quantify the chemosensitivity of primary multiple myeloma cells. Fresh BM aspirate cells were enriched for $CD138^+$ expression using Miltenyi 130-051-301 antibody-conjugated magnetic beads. Multiple myeloma cells ($CD138^+$) were seeded in Corning CellBIND 384-well plates with collagen I and previously established human-derived stroma, containing approximately 4,000 multiple myeloma cells and 1,000 stromal cells. Each well was filled with 80 μL of RPMI-1640 media supplemented with heat-inactivated FBS, penicillin/streptomycin, and patient-derived plasma (10%, freshly obtained from patients' own aspirate and filtered) and left overnight for adhesion of stroma. The next day, drugs were added using a robotic plate handler so that every drug/combination was tested at five (fixed concentration ratio, for combinations) concentrations (1:3 serial dilution) in two replicates. Negative controls (supplemented growth media with and without the vehicle control DMSO) were included, as well as positive controls for each drug (cell line MM1.S at the highest drug concentration). Plates were placed in a motorized stage microscope (EVOS Auto FL, Life Technologies) equipped with an incubator and maintained at 5% CO_2 and 37°C. Each well was imaged every 30 minutes for a total duration of up to 6 days. Cell line–positive control MM1.S cells were obtained from the ATCC and authenticated by short tandem repeat analysis once every year and *Mycoplasma* testing twice every year. These cells are supplied fresh media and split into one fourths every 2 to 3 days with a doubling time of 24 to 36 years. The number of passages of MM1.S cells used can vary between 5 and 20 passages, in which each passage lasts up to a week.

Digital image analysis algorithm

A digital image analysis algorithm (19) was implemented to determine changes in viability of each well longitudinally across 96 hours using ImageJ (RRID: SCR_003070). This algorithm computes differences in sequential images and identifies live cells with continuous membrane deformations resulting from their interaction with the surrounding extracellular matrix. These interactions cease upon cell death. By applying this operation to all 288 images acquired for each well, we quantified nondestructively, and without the need to separate stroma and myeloma, the effect of drugs as a function of concentration and exposure time.

Estimating *ex vivo* drug sensitivity: AUC

Digital image analysis computes the percent viability of multiple myeloma cells for each time point and experimental condition (drug and concentration). For each patient–drug, we have a dose–time–response surface, which is abstracted into the AUC, which is an area/integral measure of *ex vivo* response to therapy computed by taking an average of all *ex vivo* responses across all time points (first 96 hours) and concentrations (20).

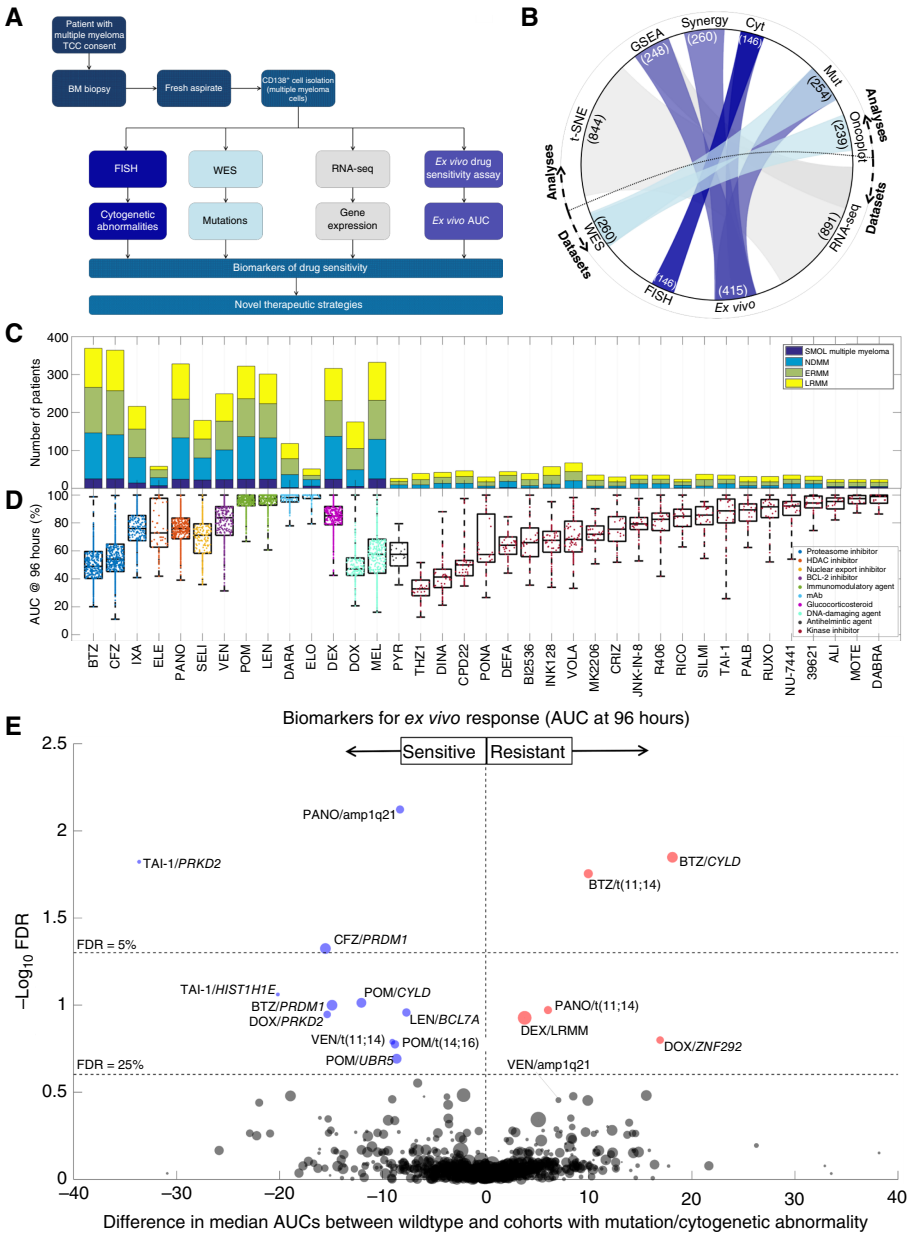

Figure 1.

Overview of the approach, *ex vivo* drug sensitivity database, and biomarkers for drug sensitivity in multiple myeloma. **A,** An overview of the proposed computational approach and integrating disparate sources of patient data, cytogenetics, WES, RNA-seq, and *ex vivo* drug sensitivity measures to synergistically identify novel therapeutic strategies in multiple myeloma. **B,** A circle plot showing the number of patients from each data source and the number of matched samples used in each type of analysis. **C,** A stacked bar plot of the number of patients in each disease state for each drug tested using the *ex vivo* drug sensitivity assay. Each bar represents the total number of samples tested with a given drug, in which most standard-of-care drugs are tested in more than 300 samples each. Samples are also denoted by four disease statuses: smoldering multiple myeloma (SMOL), newly diagnosed multiple myeloma (ND), early relapsed/refractory multiple myeloma (ER; 1–3 prior lines of therapy), and late relapsed/refractory multiple myeloma (LR; >3 lines of therapy). **D,** The *ex vivo* response measures by 96-hour AUCs of all patients tested with each drug as a box-and-whisker plot grouped by the class of the drug and arranged from most sensitive to least sensitive within each class. Disease states, cytogenetic abnormalities, and driver mutations in multiple myeloma that are associated with a statistically significant association with resistance or sensitivity to each drug are listed on the *y*-axis by the AUC. **E,** The volcano plot shows biomarkers identified for each drug by comparing *ex vivo* AUCs between patients with multiple myeloma who have the biomarker vs. those who do not. In this bubble plot, the size of the bubble represents $-\log_{10}$-adjusted *P* value, and the color signifies the extent of association with resistance (red) and sensitivity (blue) estimated by the median difference in AUCs. Multi-test correction and Benjamini–Hochberg correction were carried out across all comparisons across drugs and candidate biomarkers, which include disease states, cytogenetic abnormalities, and mutations. The *y*-axis of the volcano plot signifies statistical significance of the identified biomarker for each drug/biomarker pair, and the *x*-axis shows the median difference between the groups compared in each comparison. The drug/biomarker pairs on the left (blue) signify biomarkers for sensitivity, and the ones featured on the right (red) signify biomarkers for resistance.

WES and RNA-seq

Sample preparation

Fresh BM aspirate cells were enriched for CD138 expression using Miltenyi 130-051-301 antibody-conjugated magnetic beads. A total of 1.0×10^6 viably frozen $CD138^+$ cells were shipped for molecular analysis in the context of the ORIEN AVATAR program.

Nucleic acid extraction

For frozen tissue DNA extraction, Qiagen QIASymphony DNA purification was performed, generating a 213 bp average insert size. For frozen tissue RNA extraction, Qiagen RNAeasy Plus Mini Kit was used, generating a 216 bp average insert size.

DNA WES

Preparation of WES libraries involved hybrid capture using enhanced IDT WES and NimbleGen SeqCap EZ kits (38.7 Mb) with additional custom-designed probes for double coverage of 440 cancer genes. Library hybridization was performed at either singleplex or 8-plex and sequenced on an Illumina NovaSeq 6000 instrument, generating 100 bp paired reads. WES was performed on tumor/normal matched samples, with the normal samples covered at 100× and the tumor samples covered at 300× (additional 440 cancer genes covered at 600×) depth. Both tumor/normal concordance and gender identity quality control checks were performed. The minimum threshold for hybrid selection is >80% of bases with >20× fold coverage; ORIEN AVATAR WES libraries typically meet or exceed 90% of bases with >50× fold coverage for tumor samples and 90% of bases with >30× fold coverage for normal samples.

RNA-seq (Moffitt cohort)

RNA-seq (Moffitt cohort) was performed using Illumina TruSeq RNA Exome with single library hybridization, cDNA synthesis, library preparation, and sequencing (at either 100 or 150 bp paired reads) to a coverage of 100 M total reads/50 M paired reads.

RNA-seq (BOSTON)

RNA-seq (BOSTON) was performed on $CD138^+$ BM cells. RNA was extracted using Qiagen AllPrep RNA Mini Kit, and library preparation was performed with either TruSeq Stranded mRNA Kit (non-formalin-fixed, paraffin-embedded compatible) or SMART-Seq V4 Ultra Low Input Nextera XT Kit. Total RNA-seq was performed with 100 bp reads using an Illumina HiSeq 2500 instrument to a coverage of at least 24 M total reads/12 M paired reads.

Mutation calling: Moffitt cohort

Individual VCF files (one per sample) were converted to tab-separated format using the software vcf2tsv (https://github.com/sigven/vcf2tsv version = 0.3.4). Only gene mutation records with column value "PASS" for field "FILTER," "exonic status" as "exonic," and type "protein coding" were considered. All files were merged and formatted according to minimum requirements and processed using the R package *maftools* (RRID: SCR_024519). Mutational summaries for nonsynonymous mutations were created using *maftools* functions *oncoplot* and *plotmafSummary*, whereas "lollipop" visualizations of individual gene mutation sites were generated with *maftools* function *lollipopPlot*. Over- and under-mutated genes were assessed by the ratio of the number of mutated samples by the length of the protein in terms of the number of amino acids.

Association of *ex vivo* drug sensitivity with disease state, cytogenetic abnormalities, and driver mutations

For correlation analyses, we split the *ex vivo* patient cohort into several groups, in which the *ex vivo* drug response measure (AUC) is compared between those patients who belong to that subgroup versus those who do not via an unpaired *t* test that yields a *P* value for the comparison and a difference in median for AUCs. The *P* values are adjusted for multiple testing using the Benjamini–Hochberg method and were controlled for a FDR less than 25% (FDR ≤0.25). Supplementary Figure S1 shows a volcano plot with $-\log_{10}$ FDR on the *y*-axis and difference in median AUCs between the cohorts that have the abnormality (or mutation) versus the remaining cohort. The volcano plot depicts the statistical strength of association between a disease state/cytogenetic abnormality/mutation with *ex vivo* AUC response for each drug. We show two levels of FDR correction: a stricter FDR ≤0.05 and an acceptable threshold of FDR ≤0.25 [(similar to the threshold used by gene set enrichment analysis (GSEA)].

RNA-seq analysis: Moffitt cohort

RNA-seq tumor pipeline analysis was processed according to the workflow outlined below using GRCh38/hg38 human genome reference sequencing and GenCode (RRID: SCR_014966) build version 32.

Adapter trimming

Adapter sequences were trimmed from the raw tumor-sequencing FASTQ file. Adapter trimming via *k*-mer matching was performed along with quality trimming and filtering, contaminant filtering, sequence masking, GC filtering, length filtering, and entropy filtering. The trimmed FASTQ file was used as input to the read alignment process.

Read alignment

The tumor adapter–trimmed FASTQ file was aligned to the human genome reference (GRCh38/hg38) and the Gencode (RRID: SCR_014966) genome annotation v32 using the STAR (RRID: SCR_004463) aligner. The STAR (RRID: SCR_004463) aligner generates multiple output files used for gene fusion prediction and gene expression analysis.

RNA expression

RNA expression values were calculated and reported using estimated mapped reads, fragments per kilobase of transcript per million (FPKM) and transcripts per million mapped reads at both transcript and gene levels based on transcriptome alignment generated by STAR (RRID: SCR_004463). Gene expression data were obtained from DNAnexus files containing FPKM and transcripts per million values for 59,368 records. Among these, 19,933 were protein-coding genes, which were further analyzed; the remainder genes were discarded. For each gene/sample, we calculated $\log_2(\text{FPKM} + 10^{-3})$ and removed any genes whose values for quartiles 1 and 3 were the same (i.e., any gene must be expressed in at least 25% of samples to be considered in this analysis). The remaining 16,738 genes were z-normalized across all samples using MATLAB's (RRID: SCR_001622) function *normalize*.

RNA-seq analysis: BOSTON

RNA-seq analysis for the BOSTON (NCT03110562; ref. 15) study was performed as follows.

Trimming

Adapter trimming and quality trimming were performed on the FASTQ files using Trimmomatic (RRID: SCR_011848).

Read alignment

The adapter-trimmed FASTQ files were aligned to the human genome reference (GRCh38/hg38) using the STAR (RRID: SCR_004463) aligner.

RNA expression

FeatureCounts was used to obtain gene-level counts. After removing immunoglobulin genes, ribosomal transcripts, genes with zero counts, and genes with zero variance across all samples, the $\log_2$ counts per million mapped reads values were normalized with Voom. Covariates were identified using variancePartition (RRID: SCR_019204) and then corrected for using functions from surrogate variable analysis (SVA; RRID: SCR_002155), including ComBat (RRID: SCR_010974), to remove batch effects and library preparation bias effects.

Supervised gene sets (cancer hallmarks, Kyoto Encyclopedia of Genes and Genomes, and University of Arkansas for Medical Sciences) enriched for *ex vivo* drug resistance or sensitivity

We infer associations between *ex vivo* drug resistance or sensitivity and known biological mechanisms defined by cancer hallmarks (cancer biology), Kyoto Encyclopedia of Genes and Genomes (KEGG) pathways (cell biology, RRID: SCR_012773), and University of Arkansas for Medical Sciences (UAMS) gene sets (multiple myeloma biology) to identify cellular states that confer *ex vivo* resistance or sensitivity in multiple myeloma. We used GSEA (RRID: SCR_003199), which estimates an enrichment score (ES) for each gene set (hallmarks/KEGG/UAMS) using a running-sum statistic along the ranked list of all genes (16,738) based on the correlation between their expression and the continuous phenotypic variable (AUC). GSEA (RRID: SCR_003199) increases the running-sum statistic whenever it encounters a gene that belongs to the cluster and decreases it if it does not encounter a gene from that cluster. The maximum value of this running-sum statistic is the ES for that cluster associated with positive correlation to the continuous phenotypic variable. GSEA (RRID: SCR_003199) estimates the statistical significance of such an ES by randomly scrambling the phenotypic variable several times, and for each case, it generates a ranked gene list and the corresponding ES for the cluster of interest. All these ESs form a null distribution, which is compared with the ES for the cluster using the actual input data to estimate the nominal *P* value of enrichment. This approach is repeated for all gene sets within cancer hallmarks, KEGG (RRID: SCR_012773) pathways, or UAMS gene sets (Supplementary Fig. S2) independently, and their nominal *P* values are corrected for multiple hypothesis testing. The supervised gene sets that are enriched for resistance or sensitivity are then identified by a family-wise error rate (FWER) that is less than 5%.

Identifying transcriptomic footprints associated with *ex vivo* drug resistance or sensitivity

To unravel the transcriptomic topology of a complex disease like multiple myeloma, we used RNA-seq data from 844 patients to identify modules of coexpressing genes using a robust dimensionality reduction technique and an efficient clustering method. Z-normalized expression of 16,738 genes across 844 patients with multiple myeloma was used to identify groups of coexpressing genes that are likely to play disease-specific functional roles. Although it is typical to consider genes as variables (dimensions) and patients as observations (typically used with single-cell sequencing data to identify clones or cell types), we instead perceive patients as variables uniquely contributing to a high-dimensional multiple myeloma heterogeneity space and genes as observations that govern multiple myeloma transcriptomic topology. This leaves us with 16,738 genes spread across a massively high-dimensional (844) multiple myeloma patient space. We projected this high-dimensional data onto a two-dimensional (2D) space using t-distributed stochastic neighbor embedding (t-SNE, RRID: SCR_024305), a well-known dimensionality reduction technique that specializes in extracting features (coexpression of genes) that lie on various low-dimensional embedded manifolds (21), thereby serving as an excellent visualization tool depicting a disease-specific 2D transcriptomic map. Locations of genes on this 2D map were used to identify functional modules by using an efficient clustering algorithm called fuzzy C-means (22), which results in 500 distinct gene clusters (gene sets) of varying sizes.

We used the *ex vivo* drug sensitivity data for each drug to identify clusters that are enriched for resistance and sensitivity using GSEA (RRID: SCR_003199). GSEA (RRID: SCR_003199) estimates an ES for each cluster (gene set) using a running-sum statistic along the ranked list of all genes (16,738) based on the correlation between their expression and the continuous phenotypic variable (AUC). GSEA (RRID: SCR_003199) increases the running-sum statistic whenever it encounters a gene that belongs to the cluster and decreases it if it does not encounter a gene from that cluster. The maximum value of this running-sum statistic is the ES for that cluster associated with positive correlation to the continuous phenotypic variable. GSEA (RRID: SCR_003199) estimates the statistical significance of such an ES by randomly scrambling the phenotypic variable several times, and for each case, it generates a ranked gene list and the corresponding ES for the cluster of interest. All these ESs form a null distribution, which is compared with the ES for the cluster using the actual input data to estimate the nominal *P* value of enrichment. This approach is repeated for all 500 clusters, and their nominal *P* values are corrected for multiple hypothesis testing. The clusters that are enriched for resistance and sensitivity are then identified by a FWER that is less than 5%. These enriched clusters collectively form the transcriptomic footprint of the drug in multiple myeloma.

The transcriptomic footprints obtained using this approach are derived for SELI *ex vivo* response, DARA *ex vivo* response, SELI clinical response from BOSTON, and DARA clinical response from the Moffitt DARA cohort. Furthermore, these transcriptomic footprints have been used to carry out overrepresentation analyses using Enrichr (RRID: SCR_001575; ref. 23) to identify transcription factors (TF) and epigenetic alterations, respectively, that putatively regulate the enriched transcriptomic footprints for each drug. The transcriptomic footprints obtained using this method have also been used to inform predictor variables for the regression tree model shown to predict *ex vivo* AUC from RNA-seq data alone, in which the predicted *ex vivo* AUC was used to classify patients as "predicted sensitive" and "predicted resistant" clinically for DARA and SELI, respectively. Finally, the transcriptomic footprints derived using this approach for each of 37 drugs are used to identify pairs of drugs that have a similar enrichment pattern by correlating the ESs for each of the 500 gene clusters to identify anticorrelative drug pairs. These three downstream

analyses using the *ex vivo* derived transcriptomic footprints are detailed below in that order.

TFs and epigenetic alterations enriched for a transcriptomic footprint

The transcriptomic footprint identified from paired RNA-seq and *ex vivo* drug response data for a drug using a multiple myeloma–specific transcriptomic landscape is a collection of coexpressing gene clusters in multiple myeloma that are either enriched for sensitivity or resistance to a given drug. From this transcriptomic footprint, we derived two gene sets: genes that coexpress and are overexpressed in resistant patients and genes that coexpress among themselves and are overexpressed in sensitive patients. We subjected each of these two gene sets to overrepresentation analysis using Enrichr (RRID: SCR_001575; ref. 23) by estimating the adjusted *P* value for a one-sided Fisher exact test quantifying the significance of overlap between genes implicated in *ex vivo* resistance/sensitivity and each of ChEA 2016 (RRID: SCR_005403; for TFs that bind to genes implicated in *ex vivo* resistance/sensitivity) and Roadmap Epigenomics (RRID: SCR_008924; for epigenetic alterations that impact the expression of genes implicated in *ex vivo* resistance/sensitivity) supervised gene set databases. If the adjusted *P* value was less than 10^{-10} (Moffitt cohort) for a given test, that TF or epigenetic alteration was considered statistically significantly enriched for either resistance or sensitivity to a given drug. This significance was denoted by the diameter of the bubble in the bubble plots, whereas the intensity of the color signified the combined Enrichr (RRID: SCR_001575) score. Bubbles shown in blue represent enrichment analyses performed on genes implicated as sensitive to a given drug, whereas red bubbles signify enrichment associated with genes implicated as resistant.

Clinical response classifier using RNA-seq data and *ex vivo* transcriptomic footprints: regression tree modeling

We relied on a regression tree model that uses the median gene expression of enriched gene clusters in the transcriptomic footprint for a drug (DARA/SELI) as predictor variables (model inputs). The output of the regression tree is the *ex vivo* AUC predicted from only the RNA-seq data of a patient with multiple myeloma. The model was trained using the paired *ex vivo* AUC response (output) and the median gene expression (RNA-seq data, input) of gene clusters featured in the transcriptomic footprint. This model was used to predict *ex vivo* AUCs from gene expression alone for 22 patients with multiple myeloma treated in the clinic with a DARA-containing regimen in the Moffitt clinical cohort and 52 patients with multiple myeloma treated in the clinic with a SELI-containing regimen in the BOSTON clinical trial. The predicted *ex vivo* AUCs are used to classify patients with multiple myeloma in each cohort (DARA/SELI) as either "predicted sensitive," if their predicted AUC is in the bottom half of the cohort, or "predicted resistant," if their predicted AUC is in the top half of the cohort. These PFS of the patients from these two groups (predicted sensitive/predicted resistant) were compared using Kaplan–Meier survival plots and log-rank tests for DARA and SELI, respectively. The regression tree model for DARA was trained with 133 predictor variables, in which each predictor variable is defined by the median expression of statistically significant gene programs identified by GSEA (54 resistant and 79 sensitive). Similarly, the regression tree model for SELI was trained with 93 predictor variables, in which each predictor variable is defined by the median expression of statistically significant gene programs identified by GSEA (66 resistant and 27 sensitive). The median expression of each gene program pertains to the expression of a specific gene in that cluster, which is used as an input to each model. The regression tree modeling was implemented in MATLAB (RRID: SCR_001622) computational environment using the regression tree class available in Statistics and Machine Learning Toolbox.

Anticorrelative transcriptomic footprints to inform novel therapeutic strategies

The transcriptomic footprints derived from paired *ex vivo* AUC and RNA-seq data using GSEA (RRID: SCR_003199) result in ESs for each of the 500 clusters with genes that have a similar coexpression pattern (putatively involved in a biological process/mechanism or regulated by a common upstream TF). The GSEA (RRID: SCR_003199) enrichment for each gene cluster for every drug is given by a vector of 500 ESs and their corresponding multitest–corrected statistical significance (FWER $\leq$0.05). We imputed an ES of zero for all nonsignificant enrichments to avoid spurious associations. We correlated the 500 ESs for each pair of drugs in a clustergram, which represents drug pairs with similar enrichment patterns in red and drug pairs with anticorrelative transcriptomic footprints in blue. These anticorrelative transcriptomic footprints are of biological significance as they can target complementary mechanisms intracellularly, putatively leading to synergy from combination therapy, or target distinct tumor populations, resulting in benefit from sequential therapy.

Data availability

The Multiple Myeloma Research Foundation CoMMpass cohort RNA-seq data analyzed in this study were obtained from dbGAP under accession phs000748. WES and RNA-seq data for the Moffitt cohort analyzed in this study were generated by Aster Insights (www.asterinsights.com) in collaboration with the ORIEN (www.oriencancer.org). The raw molecular data files (FASTQ/BAM) are available upon request at https://researchdatarequest.orienavatar.com/. The processed FPKM/mutation annotation format (MAF) data files used to conduct this study are available on Synapse (RRID: SCR_006307) under Datasets at https://doi.org/10.7303/syn53254572, and the formatted input/output files to easily reproduce the analyses in this study are available on Synapse under Analyses at https://doi.org/10.7303/syn53270590. Please see the following for a detailed structure of each of these folders:

1. Datasets: https://doi.org/10.7303/syn53254572
   a. Data Key: We have compiled a comprehensive reference for all the 1,136 multiple myeloma samples used in this study, in which patient ID denotes a de-identified code for a given individual, whereas RNA, WES, and *ex vivo* IDs are sample-level identifiers. Each row denotes a biopsy/sample with the patient's demographic information, in addition to the sample IDs linking various sources of data such as RNA-seq, WES, cytogenetics, etc.
   b. *Ex Vivo* Data: This folder contains two subfolders with single-agent and combination *ex vivo* responses used in this article. The sample identifiers used here can be linked back to the Data Key folder to match with other data sources and demographic information.
   c. RNA-seq: This folder contains processed gene expression data in the form of FPKM mapped reads for 891 unique samples. The $\log_2$-transformed version and a z-normalized version of these data are also shared for ease of access.

   d. WES: This folder contains the processed MAF for 900 unique samples with mutations annotated.
2. Analyses: https://doi.org/10.7303/syn53270590
   a. t-SNE: The multiple myeloma topologic landscape used throughout this article was constructed using z-normalized RNA-seq data from an initial cohort of 844 samples shared in this subfolder along with the x and y coordinates from t-SNE used in the manuscript.
   b. *Ex Vivo* Response Paired with RNA-seq: Paired *ex vivo* response and RNA-seq data are passed through GSEA and used in analyses throughout the article. The input files for GSEA (GCT and CLS files) in standard format accepted by the software directly are shared in the Inputs subfolder. The output directories from GSEA are zipped and uploaded under the folder named Outputs.
   c. *Ex Vivo* Response Paired with Genomic Data: This folder contains associations of cytogenetic abnormalities, mutations, and disease status with *ex vivo* response to each drug reporting the nominal *P* values for an unpaired *t* test comparing the AUCs of patients with/without the event, median difference in AUCs between these two groups, and the FDR following multi-test correction.

No custom software was developed for this study except for scripts used for data formatting, filtering, and sorting. All other software from third parties are cited with version details in Materials and Methods. Scripts used for data formatting, filtering, and parsing, as well as calls to MATLAB and R libraries, are available upon request.

Results

Association of *ex vivo* drug sensitivity with clinical and genetic features of multiple myeloma

We present a computational framework integrating molecular, clinical, and *ex vivo* characteristics of BM-derived primary $CD138^+$ multiple myeloma cells, as shown in **Fig. 1A,** to discover novel therapeutic strategies in multiple myeloma. We collected a total of 1,136 samples donated by 892 patients (see Supplementary Table S1 for a summary of patient demographics): 900 unique samples from 727 patients with WES data, 891 unique samples from 725 patients with RNA-seq data, 727 unique samples from 603 patients with cytogenetic abnormalities characterized using FISH, and a total of 415 unique fresh BM aspirates from 346 patients with *ex vivo* drug sensitivity characterization. These four datasets are depicted in **Fig. 1B,** including their utilization for functional characterization described in this article, such as *ex vivo* response paired with RNA-seq ($n = 248$), WES ($n = 254$), and FISH ($n = 146$). Of the 415 samples (avatars of patients with multiple myeloma), 399 samples (from 332 patients) were treated with a total of 37 drugs (13 standard-of-care agents; see Supplementary Table S2 for more details) spanning 10 different classes (**Fig. 1C**), whereas 260 samples (from 229 patients) were treated with 51 two-drug combinations (25 standard-of-care combinations; see Supplementary Table S3 for more details).

To ensure representation of the entire disease spectrum, tested samples of patients with multiple myeloma included smoldering multiple myeloma ($n = 79$), newly diagnosed multiple myeloma ($n = 277$), early relapsed/refractory multiple myeloma (1–3 lines of therapy, $n = 339$), and late relapsed/refractory multiple myeloma (>3 lines of therapy, $n = 242$). For comparison purposes among different classes of drugs, the area under the dose–response surface (AUC; see Materials and Methods) was determined as the *ex vivo* drug response metric (**Fig. 1D**). *Ex vivo* drug sensitivity was correlated with disease state, cytogenetic abnormalities, and known multiple myeloma driver mutations (24). In **Fig. 1E**, the *x*-axis represents the difference in the medians of *ex vivo* AUCs (at 96 hours) between the wild-type and mutated (harboring a cytogenetic abnormality or disease state) groups, whereas the *y*-axis represents the $-\log_{10}$ FDR for a two-tailed unpaired *t* test comparing the two groups and subjected to multi-test correction. Consistent with clinical experience (13, 14, 25), the BCL2 inhibitor VEN was more effective in t(11;14)-bearing multiple myeloma cells. Additionally, the t(11;14) and amplification (amp)/duplication of 1q21 (three or more copies of chromosome region 1q21) were associated with resistance and sensitivity, respectively, to both the PI bortezomib (BTZ) and the pan-histone deacetylase inhibitor panobinostat (PANO; ref. 26). Consistent with recent data in multiple myeloma cell lines, we found that IMID (e.g., pomalidomide, POM) sensitivity in patient specimens was associated with increased MAF expression and/or t(14;16) (27). Additional associations were also identified between the aforementioned variables and drug response (see **Table 1**; refs. 13, 14, 27–52; Research Square rs.3.rs-125536/v1)

Although the analysis by AUCs was insightful in characterizing associations between single-agent sensitivity or resistance to multiple myeloma subgroups, it was limited by the relatively low frequency of individual driver mutations (e.g., apart from *KRAS*, *NRAS*, and *TP53*; all mutation frequencies are below 10%; Supplementary Fig. S1) or cytogenetic abnormalities in early-stage multiple myeloma, limiting the statistical power of such comparisons. To overcome these limitations, subsequent analyses focused on the transcriptome, which better informed the biology and cell-intrinsic mechanisms of multiple myeloma associated with *ex vivo* sensitivity and resistance.

Functional transcriptomic landscapes in multiple myeloma identify gene expression footprints of drug sensitivity

GSEA (53) was conducted between z-normalized gene expression (RNA-seq) and *ex vivo* drug sensitivity (AUC, average response for the entire experiment duration across all concentrations) for drugs tested in 20 or more samples, which identified cancer hallmarks (54), KEGG pathways (55) and multiple myeloma genes sets (from UAMS; ref. 56) that were enriched for *ex vivo* sensitivity and resistance (**Fig. 2A** and **B**; Supplementary Fig. S2). We have identified two groups of hallmarks/pathways associated with opposing patterns of *ex vivo* drug sensitivity in multiple myeloma: group 1 gene sets were associated with cell cycle, DNA repair, energy metabolism, and protein processing, whereas group 2 included cytokine signaling, cell adhesion, and hypoxia-related gene sets, in accordance with cell adhesion- and cytokine–mediated drug resistance mechanisms previously identified as mediators of environment-mediated drug resistance (EMDR) in multiple myeloma (57). Group 1 gene sets were associated with sensitivity to PIs, TOPO2α isomerase inhibitor doxorubicin (DOX), IMIDs, the alkylating agent melphalan (MEL), nuclear export inhibitor SELI, and PANO, as well as with resistance to DARA (an anti-CD38 mAb) and VEN. Gene sets from group 2 were associated with sensitivity to DARA, as well as resistance to PIs, the corticosteroid dexamethasone (DEX) and DOX. These observations suggest that faster cycling multiple myeloma cells would be more sensitive to cytotoxic drugs such as MEL and DOX, whereas increased expression of EMDR genes would confer resistance to PIs, yet increase sensitivity to DARA, possibly via increased

Table 1. Examples of cytogenetic abnormalities, mutations, and TFs implicated in resistance and sensitivity to various drugs.

	Drug	Feature	Phenotype	Disease	Description
Cytogenetics	VEN	t(11;14)	Sensitive	Multiple myeloma (clinical)	t(11;14) patients with multiple myeloma are sensitive to VEN (13, 14).
	VEN	Amp1q21	Resistant	Multiple myeloma	The *MCL1* locus is present in 1q21, and amp of 1q21 leads to overexpression of MCL1, which confers resistance to VEN (28).
	BTZ	t(11;14)	Resistant	Multiple myeloma (clinical)	t(11;14) results in significantly lower PFS when accompanied by the expression of CD20 in patients with multiple myeloma (29).
	PANO	t(11;14)	Resistant	Multiple myeloma	The t(11;14)-bearing U266 multiple myeloma cell line shows resistance to PANO compared with other multiple myeloma cell lines that do not possess this abnormality (30).
	POM	t(14;16)	Sensitive	Multiple myeloma	Overexpression of MAF and/or t(14;16) shows sensitivity to POM (and LEN) in multiple myeloma cell lines (27).
Mutations	BTZ	*PRDM1*	Sensitive	Mantle cell lymphoma	PRDM1 plays a key role in mantle cell lymphoma response to BTZ (31).
	BTZ	CYLD	Resistant	Multiple myeloma	CYLD K63 deubiquitinase suppresses the NF-κB pathway, and its mutation can lead to activation of NF-κB, which can confer resistance to BTZ (32).
	POM	CYLD	Sensitive	Multiple myeloma	CYLD mutation can also lead to activation of the Wnt pathway, which is implicated in cell adhesion–mediated resistance in IMIDs like LEN and POM (32).
TFs	VOLA	FOXM1	Sensitive	Esophageal adenocarcinoma	PLK1 is a cell-cycle kinase that promotes cell proliferation, which is regulated by FOXM1, and PLK1 phosphorylates FOXM1 as part of a positive feedback loop (33, 34).
	INK128	FOXM1	Sensitive	Gastric and prostate cancers	Silencing FOXM1 increased mTOR protein levels in gastric cancer cells (35), and overexpression of FOXM1 decreases mTOR signaling activity in castration-resistant prostate cancer cells (36).
	PANO	FOXM1	Sensitive	Gastric cancer and glioma	PANO decreases FOXM1 expression and induces cell-cycle arrest in gastric cancer (37).
	PYR	FOXM1	Sensitive	Multiple myeloma and glioma	Higher FOXM1 expression leads to activation of the Wnt/β-catenin pathway, which justifies the association with anthelmintic pyrvinium that blocks Wnt/β-catenin (38, 39).
	MK2206	FOXM1	Sensitive	Colorectal cancer	Activation of the PI3K-AKT signaling pathway regulates FOXM1 expression; thus, inhibiting AKT signaling reduces FOXM1 expression and leads to cell-cycle arrest (40; Research Square rs.3.rs-125536/v1).
	VEN	FOXM1	Resistant	Acute myeloid leukemia	FOXM1 knockdown decreased BCL2 mRNA and protein levels and suppressed BCL2L1 expression, leading to increased cellular dependency on BCL2 and sensitivity to VEN (41, 42).
	THZ1	FOXM1	Resistant	Breast cancer	CDK7 inhibitor resistance is associated with TGF-b/activin signaling, and FOXM1 is found to be a critical driver of TGFβ–induced endothelial-to-mesenchymal transition (43, 44).
	BTZ, CFZ, IXA	RELA	Resistant	Multiple myeloma	RELA is an NF-κB subunit, and NF-κB activity is associated with PI resistance in ultiple myeloma. The mechanism is likely regulated through the *cIAP2* gene (45, 46).
	SELI	BACH1	Resistant	Pan-cancer	BACH1 is exported from the nucleus by XPO1, and it recruits PRC2 to promote H3K27me3 modification (47, 48).
	DOX, MEL	FOXM1	Resistant	Multiple myeloma	Increased levels of FOXM1 diminish the sensitivity of multiple myeloma cells to MEL and DOX (49).
	LEN, POM	FOXM1	Resistant	Multiple myeloma	High FOXM1 expression is associated with development of resistance to LEN and cross-resistance to POM in RRMM (50).
	BI2536	FLI1	Sensitive	Ewing sarcoma	Ewing sarcoma–specific oncogenic TF EWSR1-FLI1 hijacks PRC1. PLK1 is a major upstream interacting partner of PRC1. PLK1 inhibition that can repress even chemoresistant Ewing sarcoma cells by triggering mitotic catastrophe (51).
	PONA	FOXM1	Sensitive	Chronic myeloid leukemia	Hyperactivation of the Aurora kinase A–FOXM1 axis contribute to resistance in imatinib-resistant BCR-ABL1^{+} cells. Imatinib-resistant patients displaying overexpression and hyperactivation of AKA may thus benefit from ponatinib treatment (52).

Abbreviation: RRMM, relapsed and refractory multiple myeloma.

immunogenicity (58) due to increased production of inflammatory cytokines associated with multiple myeloma–stroma cross-talk. These findings have been independently identified and characterized in cell lines by our group (59), as a cell adhesion/paracrine cytokine loop–mediated transient resistance mechanism involving fibronectin/IL6/STAT3 induced cell-cycle arrest. This mechanism may not be

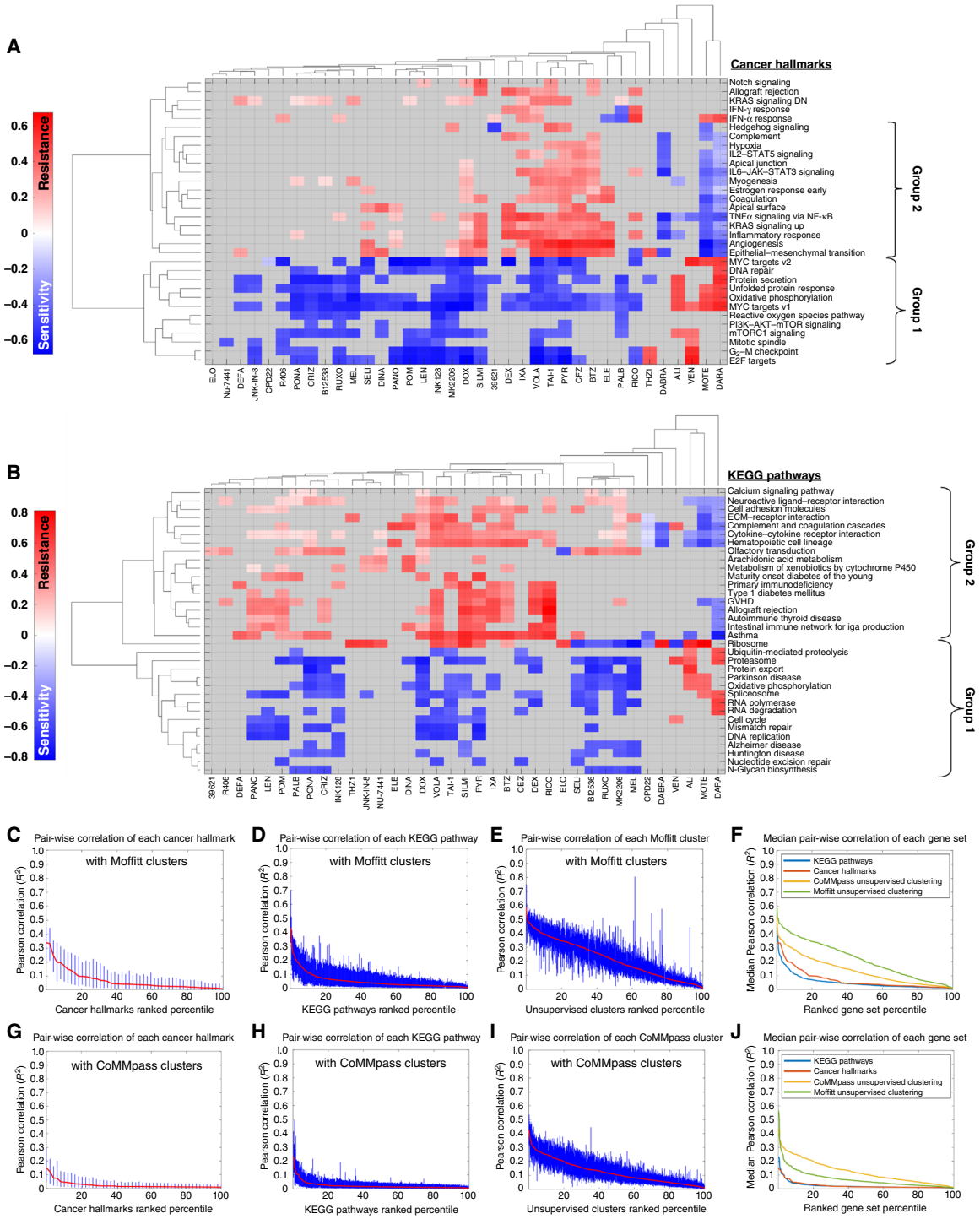

Figure 2.

GSEA identifies cancer hallmarks and KEGG pathways enriched for sensitivity and resistance. **A,** A clustergram of the normalized enrichment score computed using cancer hallmarks as supervised gene sets, in which normalized enrichment score represents the enrichment of a cancer hallmark by overexpression of genes implicated in resistance (red) or underexpression of genes implicated in sensitivity (blue) using GSEA. **B,** A clustergram using KEGG pathways as the supervised gene sets to carry out GSEA. **C–E,** All pairwise correlations (R^2) of z-normalized gene expression of any two genes within each cancer hallmark, KEGG pathway, and coexpressing Moffitt gene cluster are plotted with the ranked percentile of each gene set on *x*-axis and their respective R^2 values on the *y*-axis. Red line, median correlation within each gene set; blue bars, interquartile range of R^2. **F,** A plot showing median pairwise correlations within each gene set as a function of the ranked (by median correlation) percentile of gene sets for each of cancer hallmarks (red), KEGG pathways (blue), and Moffitt unsupervised clusters (green). **G–J,** These plots reproduce plots (**C–F**) using coexpressing gene clusters obtained from CoMMpass (36) RNA-seq data.

unique to multiple myeloma, as interdependence between cell-cycle and immunogenicity was observed and characterized in patients with breast cancer and cell lines, demonstrating that inhibition of CDK4 and CDK6 augments antigen presentation of tumor cells (60). From Supplementary Fig. S2, we note that drugs (MEL/DOX/PANO) enriched for sensitivity to group 1 gene sets for cancer hallmarks and KEGG pathways are predominantly enriched for the PR UP (proliferation) gene set in UAMS as well. However, we do not observe a strong association between any of the UAMS gene sets and EMDR gene sets (Group 2). Conversely, MS UP, known to be associated with poor prognosis in multiple myeloma, is shown to be enriched for resistance to BTZ, CFZ, and SELI, but is enriched for sensitivity to novel multiple myeloma immunotherapy agents like DARA and elotuzumab. This reinforces the need to use immunotherapies that selectively target high-risk tumor features in multiple myeloma to prolong PFS and OS of patients with multiple myeloma.

To identify putative drivers of transcriptomic dysregulation associated with drug sensitivity, we generated multiple myeloma–specific transcriptomic maps, in which genes are clustered according to their coexpression across multiple myeloma samples. Each gene cluster, after unsupervised segmentation, represented a gene set with a putative shared transcriptional regulatory mechanism (e.g., driven by a shared TF). Dimensionality reduction analysis of the z-normalized gene expression data of 844 patients with multiple myeloma was performed through t-SNE (21). This approach constructed an unbiased multiple myeloma–specific transcriptomic landscape of 16,738 multiple myeloma–expressed genes. Fuzzy c-means clustering (22) was then used to segment coexpressing gene clusters or gene programs in multiple myeloma (61). Importantly, these clusters have a higher degree of correlation of expression of their constituent genes than manually curated biological gene sets (**Fig. 2C–F**).

To validate the gene-clustering process, the analysis (**Fig. 2G–J**) was repeated using RNA-seq data from the CoMMpass (NCT01454297; ref. 62) cohort ($n = 770$ NDMM). Dimensionality reduction with t-SNE and unsupervised segmentation of the Multiple Myeloma Research Foundation dataset demonstrated higher agreement between unsupervised clusters independently identified from the two cohorts compared with the curated gene sets KEGG and cancer hallmarks. Thus, this approach identified clusters of coexpressing genes (**Fig. 3A** and **B**) with higher median pairwise Pearson correlation coefficient compared with supervised gene sets (cancer hallmarks and KEGG) in the two largest multiple myeloma RNA-seq cohorts available.

GSEA was performed on these unsupervised multiple myeloma–specific gene clusters to identify expression patterns associated with *ex vivo* resistance and sensitivity to all 37 therapeutics (Supplementary Table S2) tested. The pattern of gene clusters associated with resistance or sensitivity on the transcriptomic map was then defined as a transcriptomic "footprint" (e.g., SELI in **Fig. 3C**), in which footprints represent genes that correlate with the *ex vivo* response and that are coexpressed across samples of patients with multiple myeloma, as shown in Supplementary Fig. S3.

To illustrate how this approach can unveil drug-specific biology, we represented well-known drug target genes, as well as gene clusters identified in footprints, atop bar plots of Pearson correlation coefficients between *ex vivo* AUCs and z-normalized gene expression for 16,738 genes. Genes featured in drug resistance clusters, highlighted in red, were enriched for positive correlation with *ex vivo* AUCs, whereas genes featured in drug sensitivity clusters, highlighted in blue, were enriched for negative correlation with *ex vivo* AUCs Supplementary Figs. S4–S6. The drugs are classified into three groups, in which *ex vivo* drug sensitivity correlates with (i) gene expression of the drug targets (Supplementary Fig. S4), (ii) gene expression of upstream regulators of the drug targets (Supplementary Fig. S5), or (iii) the expression of genes involved in a biological mechanism targeted by the drug (as opposed to specific target genes, Supplementary Fig. S6). We highlight this analysis for VEN, in which *BCL2*, the target of the drug, and *CCND1*, the result of t(11;14), are shown to be highly correlated with VEN *ex vivo* sensitivity. Other genes involved in the *BCL2* family, such as *MCL1* and *BCL2L1* (*BCL-XL*), are shown to have a high correlation with VEN *ex vivo* resistance. Similarly, plots for DOX and VOLA show that the target genes *TOP2A* and *PLK1*, respectively, have high correlation with *ex vivo* sensitivity. Often the drug targets are regulated by upstream and/or pathway components. As an example, we noted that both *IL6R* and *STAT3* genes are highly negatively correlated with *ex vivo* AUCs of RUX compared with the targets *JAK1* and *JAK2* themselves. Similarly, in Supplementary Fig. S5H and S5I, bar plots for IMIDs [lenalidomide (LEN) and POM, respectively] showcasing ranked list of genes by correlation with *ex vivo* AUCs are shown, in which gene expression of *COPS7B* and *COPS8* is highly negatively correlated with both LEN and POM *ex vivo* AUCs. Notably, *COPS7B* and *COPS8* are members of the COP9 signalosome located in chromosome 2q37 and responsible for the stability of *CRBN* (target of LEN and POM), which have been shown to be associated with resistance to LEN and POM in the clinic (63). Several frequently used anticancer agents target specific biological mechanisms, with some agents having multiple modes of action. In this context, bar plots for PIs (BTZ, carfilzomib, and ixazomib; Supplementary Fig. S6A, S6B, and S6E) illustrated that expression of *PSMB5*, *PSMC7*, and *PSMD10* (genes involved in regulating proteasome subunits) consistently correlated with *ex vivo* sensitivity to each of the PIs. Interestingly, DARA has multiple modes of action in multiple myeloma involving antibody-dependent cellular cytotoxicity, antibody-dependent cellular phagocytosis, programmed cell death, and complement-dependent cytotoxicity (CDC). We note that DARA *ex vivo* sensitivity highly correlates with *C7* expression, which regulates *C5b*, a gene responsible for membrane attack complex, a key player in CDC. These findings suggest that the *ex vivo* AUCs capture DARA activity in CDC, which is also shown to correlate with increased phagocytosis (Supplementary Fig. S6C).

We employed Enrichr (23) to query publicly available databases (ENCODE/ChEA) for putative regulatory factors associated with expression of gene clusters. In **Fig. 3D**, we identified the TFs enriched for binding to genes within each gene cluster that correlated with either *ex vivo* resistance (red) or sensitivity (blue) to each drug. We carried out a similar analysis to identify epigenetic histone alterations (H3K27me3 and H3K27ac) using Roadmap Epigenomics (**Fig. 3E**) and identified coexpressing genes that are overrepresented in chromatin immunoprecipitation sequencing experiments for these epigenetic alterations in human cells (23). Among TFs, FOXM1 had the highest ES associated with sensitivity to a number of drugs of different classes, including DOX, the mTOR inhibitor INK128, PANO, POM, LEN, and the PLK1 inhibitor volasertib (VOLA). These results are consistent with FOXM1 being an important regulator of multidrug resistance in preclinical models and poor outcome in patients with multiple myeloma (64). Interestingly, *ex vivo* response to VOLA, but not BI2536, was associated with FOXM1 (**Fig. 3D**), despite both being inhibitors of PLK1, a kinase that phosphorylates and activates FOXM1, which in turn is a TF

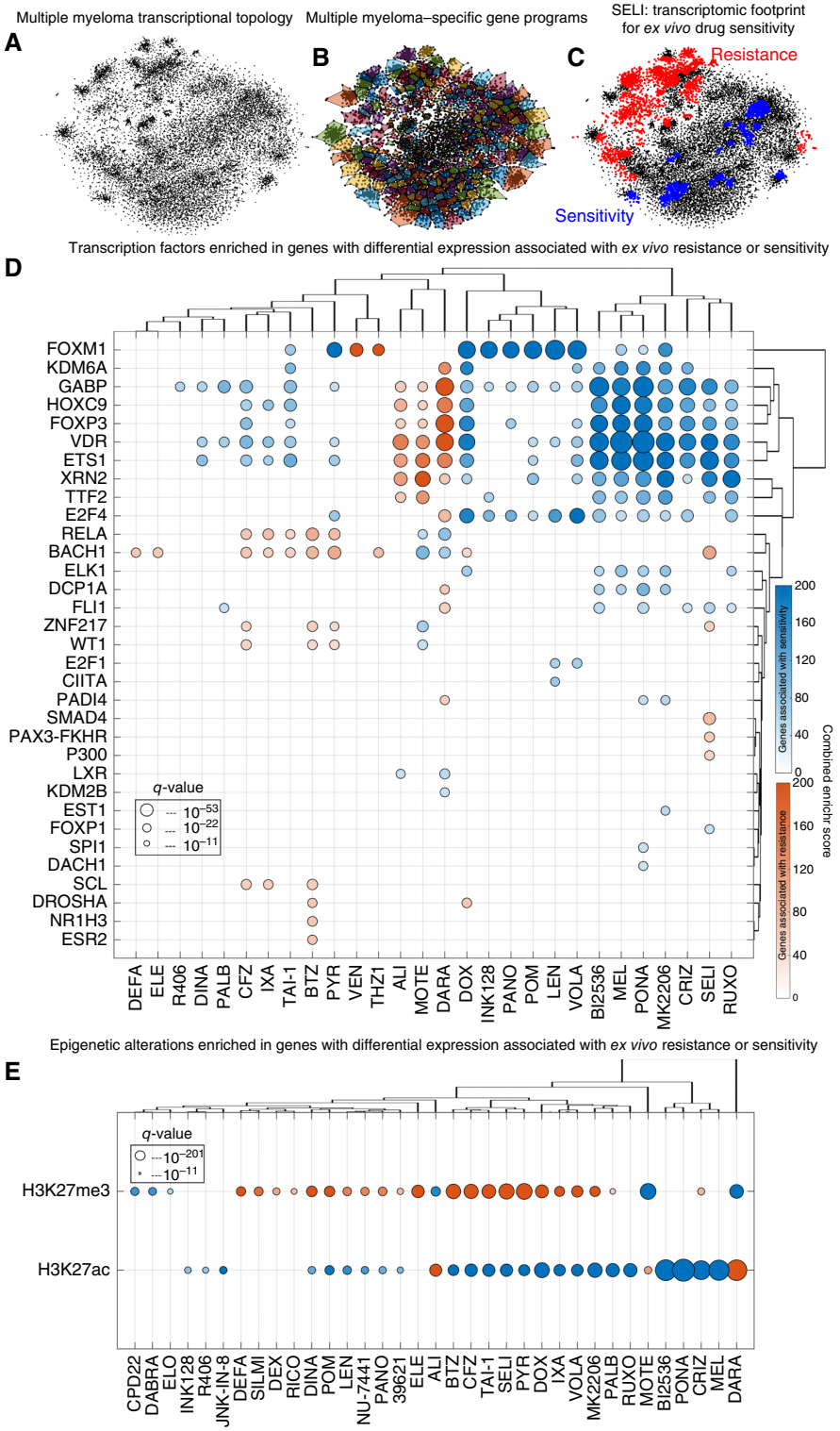

Figure 3.

The transcriptomic landscape in multiple myeloma identifies gene expression footprints of drug resistance and sensitivity. **A,** The multiple myeloma transcriptomic landscape identified by carrying out dimensionality reduction using t-SNE on normalized gene expression data from RNA-seq. **B,** Clusters of coexpressing genes identified by fuzzy c-means clustering, which serve as multiple myeloma–specific gene programs. **C,** Gene programs that are enriched for resistance (red) and sensitivity (blue) to SELI using GSEA. **D** and **E,** Bubble plots showing combined Enrichr score for sensitivity in blue and resistance in red, with the size of the bubble signifying the *P* value of the enrichment as identified by a one-sided Fisher exact test.

that positively regulates PLK1's transcription (33, 34). We believe this is due to VOLA's higher specificity to PLK1 compared with BI2536, which also targets PLK2, PLK3, MYC, and BRD4 (65), hence diluting its effect among different targets. The TFs BACH1 and RELA (an NF-κB subunit) were enriched in PI resistance, consistent with RELA-mediated induction of *cIAP2* as a mechanism of PI resistance in multiple myeloma (45, 46). Notably, the histone methyltransferase EZH2 was inversely correlated with SELI *ex vivo* resistance. This agrees with the role of EZH2, which recruits PRC2 (polycomb repressive complex-2), promoting

H3K27me3 modification and repression of gene transcription (47, 48), and a target of XPO1, which is inhibited by SELI. In accordance with the role of EZH2 activity in SELI resistance, there was a strong association between H3K27me3 genes and SELI resistance (**Fig. 3E**). Finally, six TFs/DNA-binding proteins (GABP, HOXC9, FOXP3, VDR, ETS1, and XRN2) are implicated in sensitivity to SELI, MEL, and DOX, among others, and in resistance to DARA (see **Table 1** for a detailed list of TFs implicated in *ex vivo* drug resistance and sensitivity featuring studies from the literature that corroborate our findings; refs. 33–52; Research Square rs.3.rs-125536/v1). Collectively, these data indicated that the transcriptomic footprints derived from the *ex vivo* avatars can recapitulate the biology associated with the tested therapeutics.

Development and validation of predictive biomarkers informed by transcriptomic footprints

To determine if transcriptomic footprints could serve as biomarkers that predict clinical efficacy, we examined the correlation of *ex vivo* transcriptomic footprints for DARA and SELI to footprints derived from clinical responses. DARA clinical footprints were identified using GSEA (similar to the *ex vivo* footprints) by correlating gene expression from pretreatment RNA-seq data of specimens of patients with multiple myeloma with their subsequent PFS following DARA-containing regimens (DARA/LEN/DEX, DARA/POM/DEX, or DARA/DEX) in a cohort of 22 Moffitt Cancer Center patients. SELI clinical footprints were similarly determined using a SELI-containing regimen, specifically SELI/BTZ/DEX, in a cohort of 52 patients enrolled in the BOSTON (NCT03110562; ref. 15) clinical trial–NCT0218634. For both the Moffitt (DARA) and BOSTON (SELI; ref. 15) cohorts, all samples that had pretreatment RNA-seq data available and clinical response (PFS) were considered. Statistically significant (FWER $\leq$0.05) footprints for *ex vivo* resistance (red) and sensitivity (blue) were determined by correlating gene expression with the *ex vivo* AUC for DARA (**Fig. 4A**; the same approach used in **Fig. 3C**), and statistically significant (FDR $\leq$0.25) correlations of gene expression with PFS of 22 Moffitt patients treated in the clinic were determined (**Fig. 4B**; the same approach used in **Fig. 3C,** with clinical PFS instead of *ex vivo* AUC). Similarly, gene programs were independently enriched for *ex vivo* resistance (red) and sensitivity (blue) from 81 samples of patients with multiple myeloma treated *ex vivo* with SELI (**Fig. 4C**; same as **Fig. 3C**), as well as those correlated with shorter (red) and longer PFS (blue) of 52 patients with multiple myeloma from the BOSTON (NCT03110562; ref. 15) clinical trial (**Fig. 4D**; the same approach used in **Fig. 3C,** with clinical PFS instead of *ex vivo* AUC). In addition to visual agreement between *ex vivo* and clinical footprints for both DARA (**Fig. 4A** vs. **Fig. 4B**) and SELI (**Fig. 4C** vs. **Fig. 4D**), the ESs of gene sets in both *ex vivo* (**Fig. 4A**) and clinical footprints (**Fig. 4B**) for DARA showed a high correlation (Pearson correlation coefficient, $r = 0.748$; **Fig. 4E**). Although the same correlation for SELI was less striking, it was still significant (**Fig. 4F**; Pearson correlation coefficient, $r = 0.4089$).

To assess the application of the *ex vivo* transcriptomic footprint as a predictive biomarker of clinical response (PFS) to either DARA- or SELI-based regimens, an unsupervised machine learning approach was applied to classify patients into resistant and sensitive categories (see Materials and Methods) and compare their probability of progression using Kaplan–Meier plots, **Fig. 4G** and **H**. Briefly, a regression tree model consisting of median values of enriched gene programs from the DARA and SELI *ex vivo* transcriptomic footprints were independently trained using the matched *ex vivo* AUCs and gene expression of multiple myeloma samples. We then used this model to calculate an *in silico* "*ex vivo* drug sensitivity (AUC)" for each patient in the Moffitt (DARA-treated) and BOSTON (NCT03110562, SELI-treated; ref. 15) cohorts using their RNA-seq data alone. These biomarker scores (*in silico*–calculated "*ex vivo* AUC") were then used to divide the patients into those with a high predicted AUC (predicted resistant in red) and a low predicted AUC (predicted sensitive in blue). The probability of survival computed from PFS in the Moffitt and BOSTON (15) cohorts (**Fig. 4G** and **H**) revealed a considerable (yet statistically nonsignificant) separation between the two groups despite the small sample size in each cohort and confounding effects from treatment with DEX, LEN/DEX, or POM/DEX in addition to DARA in the Moffitt cohort (transcriptomic footprint from pretreatment biopsy separates sensitive and resistant patients by PFS, log-rank test P value $= 0.156$), as well as BTZ/DEX in addition to SELI in the BOSTON (15) cohort (transcriptomic footprint from pretreatment biopsy separates sensitive and resistant patients by PFS, log-rank test P value $= 0.187$). Thus, transcriptomic footprints informed by *ex vivo* drug sensitivity data are reproduced sufficiently in clinical settings, and such transcriptomic footprints can be used as a surrogate to predict clinical outcomes.

Novel therapeutic strategies in multiple myeloma informed by transcriptomic footprints

We next tested if transcriptomic patterns associated with *ex vivo* response to anti–multiple myeloma agents enabled the identification of therapeutics that can either be sequenced or combined to optimize clinical success (longer PFS). GSEA ESs were computed for each of the 500 gene clusters (**Fig. 3B**) on the multiple myeloma transcriptomic map (**Fig. 3A**) for each agent tested *ex vivo*, in which a positive ES corresponds to resistance to a drug and a negative ES is associated with sensitivity. The similarity of transcriptomic footprints between drugs was then determined by calculating the correlation of ESs of drug pairs. The resulting Pearson correlation coefficients for every drug pair were then presented as a clustergram (**Fig. 5A**). Six clusters of correlated drugs were identified, as indicated by dashed boxes. Importantly, drug clusters 1, 2, and 3 negatively correlated with cluster 6, and cluster 4 negatively correlated with cluster 5. There are a total of 666 two-drug pairs featured in **Fig. 5A**, of which, 51 combinations (Supplementary Table S3) were tested *ex vivo* in a total of 260 samples of patients with multiple myeloma (within the 415 patient cohort), with each combination tested in at least 10 patient samples. It is important to note that the transcriptomic footprints were identified using the *ex vivo* single-agent response, whereas the combination effect was computed using the *ex vivo* combination response, which is an independent condition in each of those experiments. Supplementary Figure S7 presents a volcano plot of the 51 two-drug combinations, in which the x-axis represents the *ex vivo* combination effect (difference in the median AUC of the combination response and the additive response), the y-axis represents the $-\log_{10}$ FDR comparing the combination AUC with the additive AUC (computed from the constituent single-agent responses; ref. 10), and the size of the disc represents the number of samples tested with each combination. We use two criteria—an FDR lower than 0.05 and an *ex vivo* combination effect with a magnitude greater than 2.5%—to identify synergistic (red, combination effect greater than 2.5%) and antagonistic (blue, combination effect less than -2.5%) combinations. In **Fig. 5B**, a scatter plot is shown comparing the correlation of *ex vivo* transcriptomic footprints of drug pairs (from **Fig. 5A**) on the y-axis and their *ex vivo*

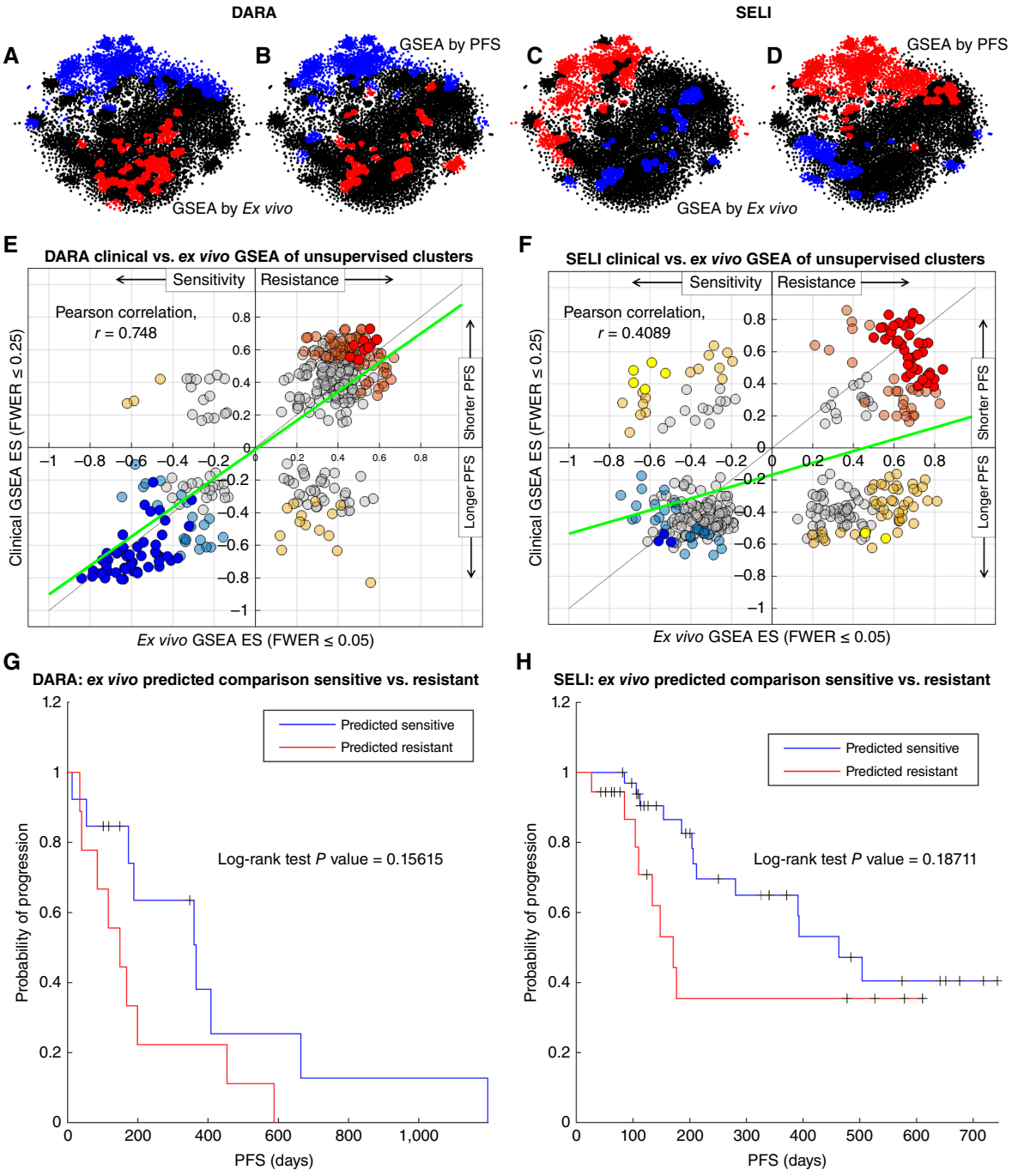

Figure 4.

Validation of transcriptomic footprints identified for *ex vivo* drug sensitivity and resistance. **A** and **B,** Enriched gene programs for *ex vivo* resistance (red) and sensitivity (blue) for DARA (**A**) and the gene sets enriched for clinical response (PFS; **B**). **C** and **D,** Comparison of enriched gene programs from *ex vivo* (**C**) and clinical response (PFS; **D**) for SELI. **E** and **F,** Correlation of GSEA ESs for gene programs that are featured in both *ex vivo* and clinical gene sets for DARA (**E**) and SELI (**F**), respectively. Gray represents nonsignificant gene sets, and yellow represents gene sets that GSEA suggested opposing enrichments for that gene cluster in *ex vivo* and clinical contexts. FWER, family-wise error rate. **G,** Median gene expressions of enriched gene programs identified from *ex vivo* response (**A** and **C**) are used to predict the AUC using a regression tree model. This predicted AUC from gene expression is used to classify patients as sensitive and resistant, whereas the PFS for these patients (who received DARA in the clinic immediately after the biopsy used for RNA-seq) is used to compare probability of progression using a Kaplan–Meier plot. **H,** Kaplan–Meier plot showing the ability of *ex vivo*–identified gene programs to classify patients clinically for SELI.

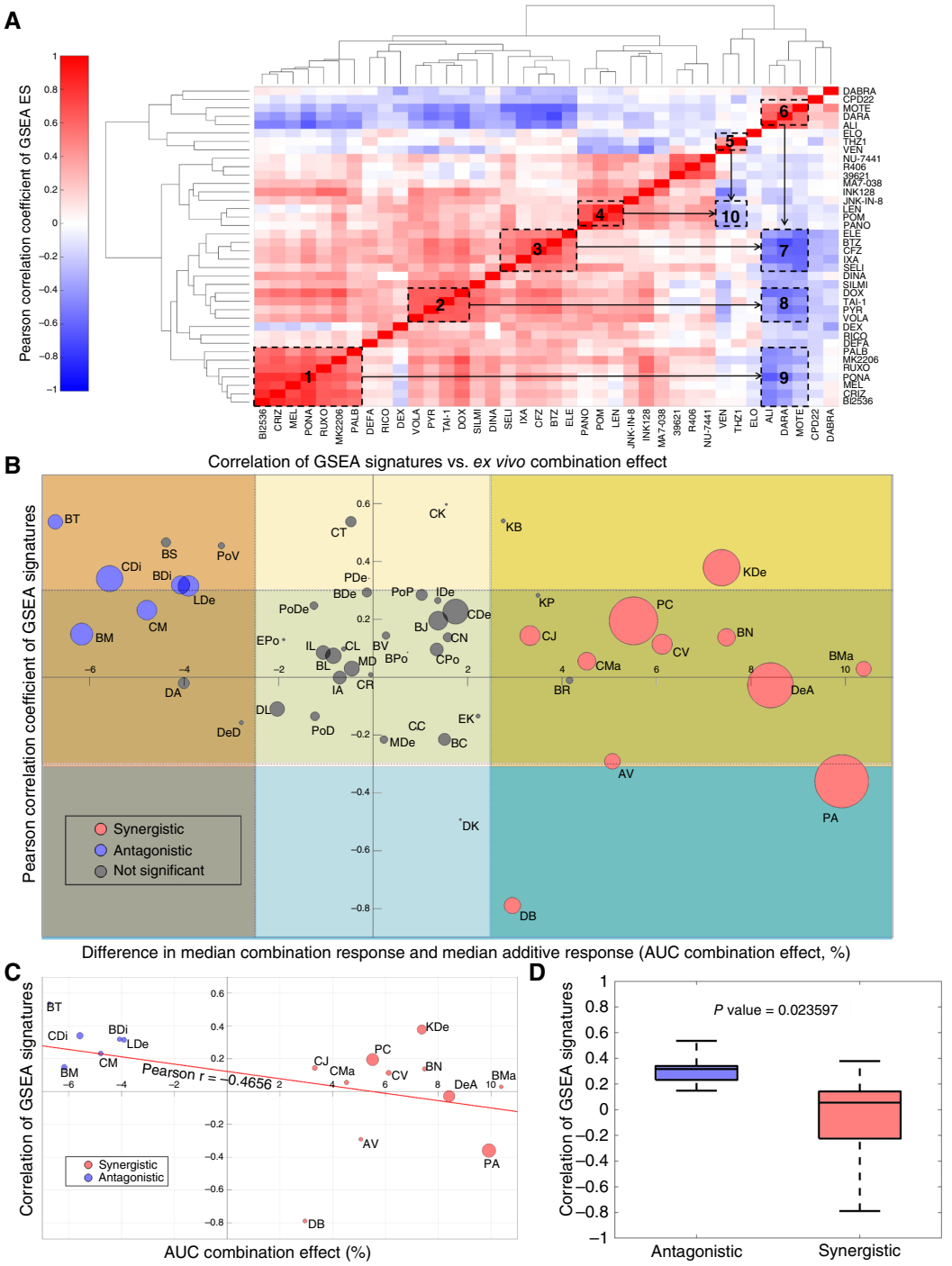

Figure 5.

Correlations of GSEA ESs suggest novel therapeutic strategies. **A,** Clustergram of correlations of GSEA ESs for each cluster for every pair of drugs tested *ex vivo* identifies pairs of drugs that have positively correlated and negatively correlated transcriptomic footprints. **B,** A scatter plot showing the relationship between correlation of GSEA transcriptomic footprints and differences in the median of combination and additive responses (AUC combination effect). Each bubble (or circle) represents a two-drug combination that has a corresponding pairwise correlation between the constituent single agents in **A**. The blue and red bubbles represent statistically significant synergistic and antagonistic combinations, respectively, whereas the gray bubbles represent a nonsignificant combination effect or additivity. **C,** A scatter plot showing only statistically significant two-drug combinations from **B** or Supplementary Fig. S2, in which the correlation of GSEA transcriptomic footprints and the AUC combination effect are subjected to Pearson linear correlation. **D,** A box-and-whisker plot showing the difference in correlation of GSEA transcriptomic footprints between statistically significant synergistic and antagonistic combinations from **B** or Supplementary Fig. S2. The correlations from the two groups were subjected to a two-tailed unpaired *t* test, and the *P* value for this comparison is shown.

combination effect (from Supplementary Fig. S7) on the *x*-axis, with the size of the disc representing the statistical significance of the combination effect ($-\log_{10}$ FDR; shown on the *y*-axis from Supplementary Fig. S7).

Notably, a negative correlation of transcriptomic footprints favors synergistic combinations, whereas a positive correlation could correspond to either synergism or antagonism. Linearly correlating the statistically significant *ex vivo* combination effects with their corresponding correlations of transcriptomic footprints (**Fig. 5C**) resulted in a Pearson correlation coefficient (r) of -0.4656, indicating that anticorrelative transcriptomic footprints are more likely associated with synergism. This notion was supported by comparing the correlation of transcriptomic footprints for statistically significant antagonistic/synergistic combinations featured in **Fig. 5D** using an unpaired two-tailed t test, which yielded a P value of 0.023597, underscoring the fact that statistically significant antagonistic combinations have a higher and always a positive correlation of transcriptomic footprints.

Given these properties, we focused on anticorrelative combinations in **Fig. 5B**, in which a threshold of -0.3 denotes significantly anticorrelative transcriptomic footprints. This analysis identified three drug pairs having such features: DARA/BTZ, PANO/VEN (PA), and DARA/SELI. The most anticorrelative drug pair, DARA/BTZ, along with DEX, is an approved combination for multiple myeloma that has shown great efficacy in patients with newly diagnosed multiple myeloma in a phase III clinical trial when compared with patients treated with BTZ and DEX alone (66). The drug pair PA has the highest statistical significance in *ex vivo* synergy (Supplementary Fig. S7), and although there are currently no ongoing clinical studies involving this combination, preclinical studies have shown synergism between these two agents (67, 68). The synergism of PA is also exemplified in the association of *ex vivo* drug sensitivity and cytogenetic abnormalities (**Fig. 1E**), which shows that PANO is associated with *ex vivo* sensitivity in patients with amp of 1q21 and to resistance in t(11;14)-positive patients with multiple myeloma. VEN, on the other hand, is associated with *ex vivo* (and clinical) sensitivity in t(11;14)-positive patients and to resistance (relatively lower significance, FDR ~40%) in patients with amp of 1q21. Such an inverse association with t(11;14) and amp of 1q21 is also supported by the biological rationale for simultaneously targeting two key antiapoptotic proteins, BCL2 and MCL1 (69), in which t(11;14) patients are associated with high BCL2 expression (70) and amp of 1q21 leads to overexpression of MCL1 as its locus is present in chr1q21 (28). Supplementary Figure S8A shows that BCL2 and CCND1 expressions correlate with *ex vivo* VEN sensitivity, whereas MCL1 and BCL2L1 expressions correlate with *ex vivo* resistance. Conversely, Supplementary Fig. S8B shows the opposite relationship for PANO. These opposing roles of BCL2 and MCL1 expressions agree with opposite associations between t(11;14) (sensitivity for VEN and resistance for PANO) and amp/gain 1q21 (resistance for VEN and sensitivity for PANO) cytogenetic abnormalities in **Fig. 1E** and anticorrelative transcriptomic footprints in **Fig. 5A** and are shown to be synergistic in Supplementary Fig. S7. Supplementary Figure S8C–S8F present networks of upstream TFs that bind to the promoter regions of the genes implicated in resistance/sensitivity for VEN/PANO. We note that the TF network for VEN resistance in Supplementary Fig. S8C and PANO sensitivity network in Supplementary Fig. S8F features similar TFs like E2F4, FOXM1, SIN3A, and IRF3. Despite a missing overlap between PANO resistance network (EZH2 and SUZ12) and VEN (BCL3, RELA, and REST) sensitivity network. Supplementary Fig. S8A and S8B demonstrates that BCL2 and CCND1 expressions can be used as effective biomarkers for VEN sensitivity and PANO resistance. The third drug pair with inversely correlated transcriptomic footprint, DARA/SELI, trends toward synergism, although this is not statistically significant, possibly due to a small sample size of this cohort ($n = 13$).

Anticorrelative transcriptomic footprints support sequential DARA–SELI therapy

As genes associated with sensitivity to a specific drug are implicated in resistance to another, we reasoned that anticorrelative transcriptomic footprints could also inform the benefit of sequential therapies by creating an evolutionary double bind (71). We considered SELI (cluster 3; from **Fig. 5A**) and DARA (cluster 6; from **Fig. 5A**) as candidates due to the anticorrelative transcriptomic footprints for *ex vivo* sensitivity and resistance of DARA (**Fig. 6A**; same as **Fig. 4A**) and SELI (**Fig. 6B**; same as **Figs. 3C** and **4C**), in which the enriched gene sets of cancer hallmarks for *ex vivo* drug response for each of the two drugs are also anticorrelative (**Fig. 6C**). The choice for studying this drug pair was also motivated by a subgroup analysis from the phase 3 BOSTON trial (NCT03110562; ref. 15), in which patients with multiple myeloma treated with DARA in a prior line of therapy showed further improved PFS in the SELI/BTZ/DEX (XVd) arm versus the BTZ/DEX (Vd) arm with a HR of 0.49 (95% CI, 0.13–1.84; ref. 28). Furthermore, this improvement in PFS was higher in patients treated with DARA in a prior line of therapy when compared with the improvement in PFS between XVd and Vd arms for the entire cohort (HR, 0.7; 95% CI, 0.53–0.93; refs. 15–18). Based on the anticorrelative transcriptomic profiles and this subgroup analysis, we hypothesized that patients who received DARA in an immediate prior line would benefit more from a SELI-based regimen than those who received it in an earlier prior line. To investigate this clinically, we analyzed two independent SELI-based trials. Notably, PFS in triple-class refractory patients (i.e., all patients had received an anti-CD38 mAb) from two arms of the STOMP (NCT02343042; refs. 16, 17) clinical trial [SELI/POM/DEX (XPd) and SELI/CFZ/DEX (XKd)] and the XPORT-MM-028 (NCT04414475, XVd) clinical trials (Supplementary Table S4; ref. 18) revealed that the PFS of patients exposed to an anti-CD38 mAb in their immediate prior line was higher in both the STOMP (NCT02343042; 15 vs. 8.9 months; log-rank test P value $= 0.096$; refs. 16, 17) and XPORT-MM-028 (NCT04414475; NE vs. 3.5 months; log-rank test P value $= 0.057$; ref. 18) trials (**Fig. 6D** and **E**). Collectively, these clinical data provide a strong rationale for sequencing SELI after DARA based on *ex vivo* functional transcriptomics and correlative science.

Discussion

Despite significant increases in the number of approved therapies leading to a steady improvement in the 5-year survival rate, multiple myeloma remains all but incurable. We and others have reasoned that improving multiple myeloma clinical outcomes with currently available therapeutics might be achieved through optimal therapeutic interventions using predictive biomarkers (9, 10, 18). Whereas diagnostic and prognostic biomarkers are integrated into clinical utilization in multiple myeloma (4), predictive biomarkers are lacking. In this study, using functional transcriptomics as defined by *ex vivo* drug screening as patient avatars (surrogates for clinical response) and paired molecular data, we identify critical multiple myeloma biology and predictive molecular biomarkers.

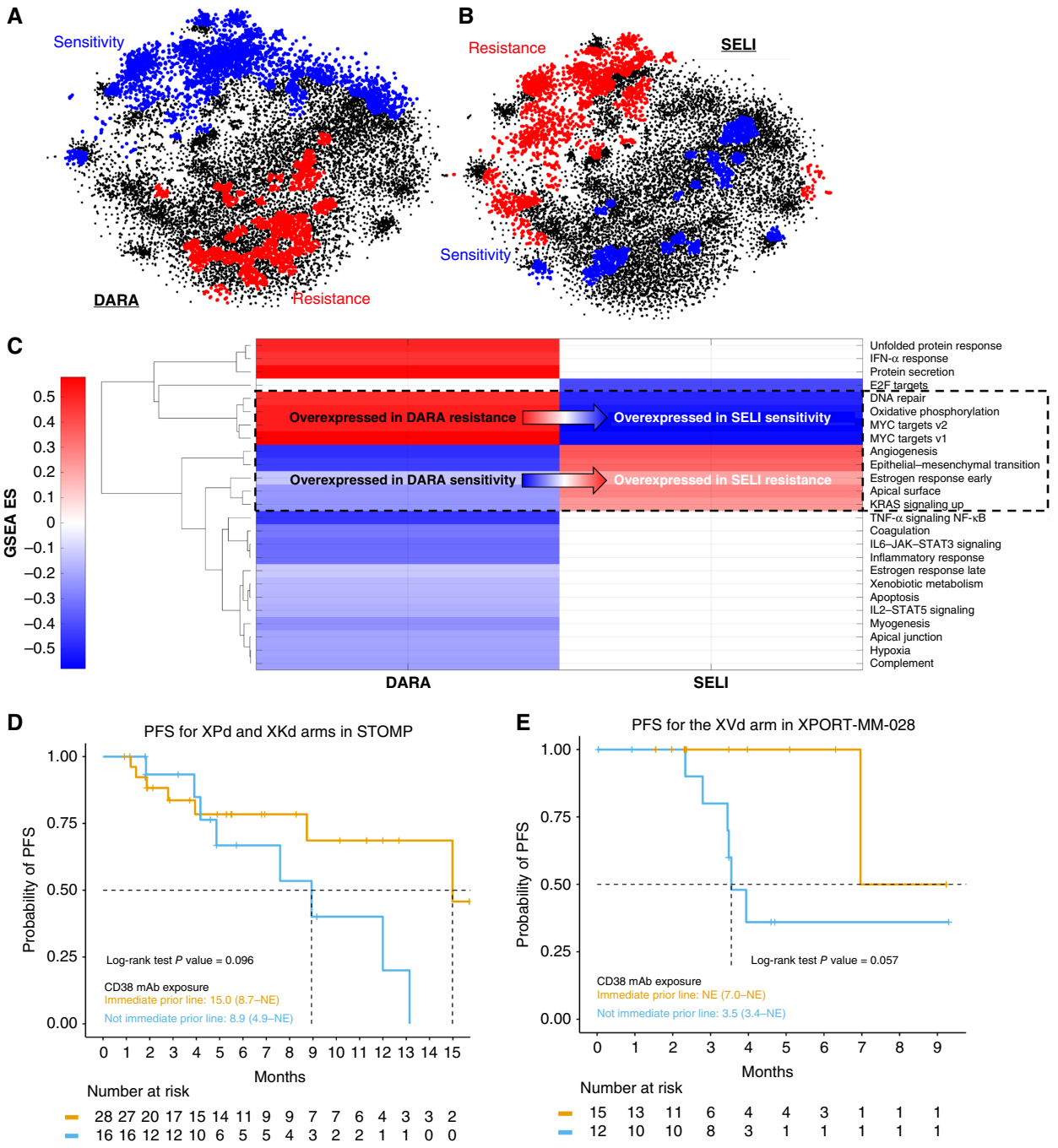

Figure 6.

SELI and DARA: a novel sequential therapy informed by multiple myeloma functional transcriptomics. **A** and **B,** A clustergram of enriched cancer hallmarks for *ex vivo* drug sensitivity or resistance to SELI and DARA. **C,** The anticorrelative *ex vivo* transcriptomic footprints of SELI and DARA. **D** and **E,** The probability of PFS compared between the two groups shows improved survival in patients treated with a SELI-based regimen combined with a DARA-based regimen as an immediate prior line in STOMP and XPORT-MM-028.

Importantly, these findings were validated by molecular and clinical data from independent clinical trials.

The findings reported herein are based on robust analyses of patient-derived multiple myeloma cells from 415 patients who were screened *ex vivo* with 37 standard-of-care, experimental, and preclinical drugs, which were tested in a minimum of 20 samples. Within this larger cohort, 265 samples were characterized according to FISH cytogenetics, RNA-seq, and WES. Integrating these data confirmed previously identified predictive biomarkers [e.g., t(11;14) predicts VEN response and t(14;16) and/or MAF expression is

associated with IMID sensitivity, as demonstrated in a recent study in a panel of cell lines, refs. 25, 27] as well as new potential biomarkers for further investigation (**Table 1**). However, identification of molecular biomarkers such as the t(11;14) or t(14;16) for the majority of multiple myeloma agents is limited by multiple myeloma's inherently low mutational/cytogenetic frequency (72). Thus, we focused our efforts on the multiple myeloma transcriptome, in which GSEA revealed two general groups that are differentially expressed according to *ex vivo* resistance and sensitivity (cell cycle/DNA repair/energy metabolism/protein- and EMDR-related, respectively) that have opposing patterns of correlation between gene expression and *ex vivo* response to three groups of in-clinic multiple myeloma drugs (IMIDs/SELI/MEL, PIs/DOX/DEX, and DARA).

Importantly, the transcriptomic landscape of multiple myeloma revealed clusters of coexpressing genes across this multiple myeloma patient cohort, and GSEA analysis of 37 drugs relative to these gene clusters generated transcriptomic footprints that informed transcriptomic drivers of *ex vivo* drug response and predictive biomarkers. As a proof of principle, the SELI transcriptomic footprint derived from *ex vivo* response was compared with transcriptomic footprints obtained from clinical response to a SELI-based regimen in a cohort of 52 patients enrolled in the BOSTON trial (NCT03110562; ref. 15) and a DARA-based regimen in a cohort of 22 patients from Moffitt Cancer Center. This comparison demonstrated positive correlation of ESs between *ex vivo* and clinical transcriptomic footprints for both SELI and DARA. Furthermore, the gene clusters obtained from the transcriptomic footprint can be used to train a regression tree model that predicts *ex vivo* drug sensitivity from gene expression data alone, and this RNA-seq based model sufficiently identifies patients with longer PFS (predicted as sensitive; blue in **Fig. 4G** and **H**) and shorter PFS (predicted as resistant, red in **Fig. 4G** and **H**).

We have defined the term transcriptomic footprint as the collective of gene sets whose ESs correlate with resistance or sensitivity (*ex vivo*/AUC or clinical/PFS) to a single drug. Thus, we defined similarity between pairs of drugs as a metric of agreement between their footprints, generating a list of positively, weakly, and negatively correlated drug pairs, and investigated whether these would be a predictor of *ex vivo* synergy. Positively correlated drug pairs were identified as most likely antagonistic with some notable exceptions, whereas negatively correlated drug pairs were found to be synergistic or additive. Finally, supporting the clinical accuracy of these models, a correlation matrix of the transcriptomic footprints for each of the 37 drugs was created to identify pairs of drugs with anticorrelative transcriptomic profiles, in which we hypothesized that therapeutics with anticorrelative profiles could also be candidates for sequential therapy (i.e., they inform the choice of follow-up regimen upon relapse), as the biology associated with resistance to one drug is associated with sensitivity to the other. SELI and DARA were tested as candidates for this approach using data from two clinical trials, STOMP (NCT02343042; refs. 16, 17) and XPORT-MM-028 (NCT04414475; ref. 18), in which patients treated with a SELI-based regimen who received DARA-therapy in an immediate prior line had deeper responses and longer PFS. Collectively, these data support the rationale for the use of predictive biomarkers defined by this functional transcriptomics platform to inform novel therapeutic strategies with current and future multiple myeloma therapies.

Analyses of the transcriptomic footprints that drive clinical benefit seen with DARA–SELI sequential therapy (**Fig. 5C** and **D**) revealed that gene clusters that positively correlated with *ex vivo* SELI resistance, and conversely *ex vivo* DARA sensitivity, are enriched for immune/microenvironment-mediated pathways (e.g., IL2/STAT5, IL6/JAK/STAT3) and are complement, and thus they are expected to be involved in multiple myeloma immune surveillance. Additionally, enrichment analysis of human-derived chromatin immunoprecipitation sequencing databases suggest H3K27me3 histone modifications control transcription of these gene sets (**Fig. 4C**), an observation we have confirmed by single-cell Assay for Transposase-Accessible Chromatin using sequencing in primary multiple myeloma samples (61). Finally, SELI inhibits XPO1 activity, which directs nuclear export of multiple TFs, including EZH2, which recruits PRC2 and promotes H3K27me3 modifications (47, 48). Collectively, these findings support a model whereby DARA-refractory multiple myeloma cells epigenetically suppress immunogenic genes through H3K27me3, which in turn makes them more vulnerable to disruption of nuclear export machinery that is needed to maintain gene suppression. Ongoing studies will further test these predictions.

Using a robust multiple myeloma patient database and a new unsupervised approach to infer mechanisms driving drug response, in the form of drug-specific transcriptomic footprints, the findings presented herein establish how such footprints can generate patient-specific predictive biomarkers and inform the design and optimize the outcomes of evolution-inspired clinical trials. We anticipate that this approach could accelerate the development of experimental preclinical drugs and clinical therapies (including immunotherapies) by increasing the probability of success, which is estimated to be 35.5% in phase III clinical trials and much lower in earlier stages (73). Accordingly, we predict that by identifying novel therapeutic strategies informed by data-driven approaches as those described herein, the success of oncology drug development and the use of standard-of-care therapies can be markedly improved.

Authors' Disclosures

P.R. Sudalagunta reports personal fees from FORUS Therapeutics Inc. outside the submitted work; in addition, P.R. Sudalagunta has a patent for "A model of clinical synergy in cancer, PCT/US2020/062232 (WO/2021/108551-A1)" pending, a patent for "A multiomic approach to modeling of gene regulatory networks in multiple myeloma, PCT/US2022/024217 (WO/2022/217136-A1)" pending, and a patent for "Altering epigenetic landscapes control progression and refractory disease states in multiple myeloma, PCT/US2023/078667 (WO/2024/097981)" pending. R.R. Canevarolo reports a patent for WO2024097981A1 pending to Moffitt Cancer Center, a patent for WO2022217136A1 pending to Moffitt Cancer Center, and a patent for WO2021108551A1 pending to Moffitt Cancer Center. M.B. Meads reports a patent for "A model of clinical synergy in cancer," PCT/US2020/062232 (WO/2021/108551-A1), priority date November 25, 2019, pending to H. Lee Moffitt Cancer Center and Research Institute, a patent for "A multiomic approach to modeling of gene regulatory networks in multiple myeloma," PCT/US2022/024217 (WO/2022/217136-A1), priority date October 04, 2021, pending to H. Lee Moffitt Cancer Center and Research Institute, and a patent for "Altering epigenetic landscapes control progression and refractory disease states in multiple myeloma," PCT/US2023/078667 (WO/2024/09798-A1), priority date March 11, 2022, pending to H. Lee Moffitt Cancer Center and Research Institute. O. Hampton reports O. Hampton was a paid employee of Aster Insights while conduction of research. J.K. Teer reports grants from the NIH during the conduct of the study; in addition, J.K. Teer has a patent for Negative Information Storage Model issued. B.D. Shah reports grants, personal fees, and other support from Kite/Gilead, other support from Servier and Pepromene Bio, personal fees and other support from Jazz, and personal fees from Novartis, Deciphera, Takeda, Beigene, Pfizer, Bristol Myers Squibb, Amgen, Adaptive, Lilly/Loxo, from Autolus, and Syndax outside the submitted work. L. Hazlehurst reports being a cofounder of Modulation Therapeutics, but this work is not related to the current pipeline at Modulation Therapeutics. Y. Chai reports other support from Karyopharm Therapeutics during the conduct of the study. A. DeCastro reports was a former

employee of one of the therapeutics tested in the study (Karyopharm Therapeutics). E.M. Siegel reports grants from the NIH NCI outside the submitted work. M. Alsina reports grants from Bristol Myers Squibb and other support from Janssen and Sanofi outside the submitted work. T. Nishihori reports other support from Novartis and Karyopharm Therapeutics outside the submitted work. J.L. Cleveland reports grants from the NCI/NIH during the conduct of the study. W. Dalton reports grants from Karyopharm Therapeutics during the conduct of the study and personal fees from AsterInsights outside the submitted work. C.J. Walker reports other support from Karyopharm Therapeutics during the conduct of the study. Y. Landesman used to work for Karyopharm Therapeutics and still holds stock of the company. R. Baz reports personal fees and other support from Janssen, other support from Abbvie, Regeneron, and Bristol Myers Squibb, and personal fees from Pfizer and Cellectar outside the submitted work. A.S. Silva reports a patent for A.S. Silva, K.H. Shain, P.R. Sudalagunta, R.R. Canevarolo, and M.B. Meads, "A model of clinical synergy in cancer," PCT/US2020/062232 (WO/2021/108551-A1), priority date November 25, 2019, issued, a patent for A.S. Silva, K.H. Shain, P.R. Sudalagunta, R.R. Canevarolo, and M.B. Meads, "A multiomic approach to modeling of gene regulatory networks in multiple myeloma," PCT/US2022/024217 (WO/2022/217136-A1), priority date October 04, 2021, pending, and a patent for A.S. Silva, K.H. Shain, P.R. Sudalagunta, R.R. Canevarolo, and M.B. Meads, "Altering epigenetic landscapes control progression and refractory disease states in multiple myeloma," U.S. Provisional Application No. 63/422,106, priority date March 11, 2022, pending. K.H. Shain reports grants and personal fees from Karyopharm Therapeutics during the conduct of the study and grants from Abbvie and personal fees from Bristol Myers Squibb, Janssen, Amgen, Regeneron, Adaptive, and Sanofi outside the submitted work; in addition, K.H. Shain has a patent for 10110-243US1 pending and a patent for 10110-363WO1 issued. No disclosures were reported by the other authors.

Authors' Contributions

P.R. Sudalagunta: Conceptualization, data curation, software, formal analysis, validation, investigation, visualization, methodology, writing–original draft, project administration, writing–review and editing. **R.R. Canevarolo:** Conceptualization, data curation, formal analysis, validation, visualization, methodology, writing–original draft, writing–review and editing. **M.B. Meads:** Conceptualization, resources, data curation, supervision, validation, investigation, visualization, writing–original draft, writing–review and editing. **M. Silva:** Resources, data curation, validation, writing–review and editing. **X. Zhao:** Resources, data curation, validation, investigation, visualization, writing–original draft, writing–review and editing. **C.L. Cubitt:** Resources, data curation, writing–review and editing. **S.S. Sansil:** Resources, data curation, writing–review and editing. **G. DeAvila:** Data curation, writing–review and editing. **R.R. Alugubelli:** Data curation, software, visualization, writing–review and editing. **R.T. Bishop:** Resources, data curation, validation, investigation, writing–review and editing. **A. Tungesvik:** Resources, data curation, writing–review and editing. **Q. Zhang:** Resources, Data curation, software, formal analysis, writing–review and editing. **O. Hampton:** Resources, data curation, software, formal analysis, supervision, writing–review and editing. **J.K. Teer:** Resources, data curation, software, formal analysis, validation, investigation, writing–original draft, writing–review and editing. **E.A. Welsh:** Resources, data curation, software, formal analysis, writing–review and editing. **S.J. Yoder:** Resources, data curation, software, formal analysis, supervision, writing–review and editing. **B.D. Shah:** Resources, data curation, supervision, funding acquisition, validation, writing–review and editing. **L. Hazlehurst:** Resources, data curation, supervision, validation, writing–review and editing. **R.A. Gatenby:** Resources, data curation, supervision, funding acquisition, writing–review and editing. **D.R. Van Domelen:** Data curation, software, formal analysis, validation, visualization, writing–review and editing. **Y. Chai:** Data curation, software, formal analysis, validation, visualization, writing–review and editing. **F. Wang:** Data curation, software, formal analysis, visualization, writing–review and editing. **A. DeCastro:** Data curation, software, formal analysis, supervision, visualization, writing–review and editing. **A.M. Bloomer:** Resources, data curation, validation, writing–review and editing. **E.M. Siegel:** Resources, data curation, validation, writing–review and editing. **C.C. Lynch:** Conceptualization, resources, data curation, supervision, validation, investigation, writing–review and editing. **D.M. Sullivan:** Conceptualization, Resources, data curation, supervision, funding acquisition, writing–review and editing. **M. Alsina:** Conceptualization, resources, data curation, supervision, funding acquisition, validation, investigation, writing–review and editing. **T. Nishihori:** Resources, data curation, validation, investigation, writing–review and editing. **J. Brayer:** Resources, data curation, supervision, validation, investigation, writing–review and editing. **J.L. Cleveland:** Conceptualization, resources, data curation, formal analysis, supervision, funding acquisition, validation, investigation, visualization, writing–original draft, writing–review and editing. **W. Dalton:** Conceptualization, resources, data curation, software, supervision, funding acquisition, validation, investigation, writing–review and editing. **C.J. Walker:** Conceptualization, resources, data curation, software, formal analysis, validation, investigation, visualization, writing–original draft, writing–review and editing. **Y. Landesman:** Conceptualization, resources, data curation, software, formal analysis, supervision, validation, investigation, visualization, writing–review and editing. **R. Baz:** Conceptualization, resources, data curation, supervision, funding acquisition, validation, investigation, visualization, methodology, writing–review and editing. **A.S. Silva:** Conceptualization, resources, data curation, software, formal analysis, supervision, funding acquisition, validation, investigation, visualization, methodology, writing–original draft, project administration, writing–review and editing. **K.H. Shain:** Conceptualization, resources, data curation, software, formal analysis, supervision, funding acquisition, validation, investigation, visualization, methodology, writing–original draft, project administration, writing–review and editing.

Acknowledgments

The authors sincerely thank the patients with multiple myeloma and their families for donating their samples for research purposes. The authors also thank the members of the K.H. Shain, A.S. Silva, and J.L. Cleveland laboratories and the Pentecost Myeloma Research Center for scientific discussions. This research was made possible through the Oncology Research Information Exchange Network Avatar Project in collaboration with Aster Insights (formerly known as M2Gen) and the Total Cancer Care protocol at the H. Lee Moffitt Cancer Center and Research Institute, an NCI-designated Comprehensive Cancer Center (P30-CA076292). The authors are also grateful for the expert assistance and service of Proteomics and Metabolomics, Molecular Genomics, Cancer Pharmacokinetics and Pharmacodynamics, Comparative Medicine, Flow Cytometry, and Biostatistics and Bioinformatics departments of Moffitt Cancer Center and Aster Insights (formerly M2Gen). This work was supported by philanthropic support from the Pentecost Myeloma Research Center (to R. Baz, K.H. Shain, A.S. Silva, M. Alsina) and in part by the Moffitt Cancer Center Physical Sciences in Oncology (PSOC) grant 1U54CA193489-01A1 (K.H. Shain, A.S. Silva, R.J.G, J.L. Cleveland, and R.A. Gatenby), a Moffitt Cancer Center's Team Science grant (A.S. Silva, K.H. Shain), a Miles for Moffitt Foundation grant (A.S. Silva), a 2021 Multiple Myeloma Research Foundation Research Fellowship Award (P.R. Sudalagunta), Florida Department of Health, Public Health Research, Biomedical Research Program (K.H. Shain), the Cortner-Couch Endowed Chair for Cancer Research from the University of South Florida School of Medicine (J.L. Cleveland), 1R01CA195727 (L. Hazlehurst and A.S. Silva), Cancer Center Support Grant P30-CA076292 to the Moffitt Cancer Center, and personal donations from Lisa France Kennedy (J.L. Cleveland). Steve Mitchell, Principal Scientific Writer, Karyopharm Therapeutics Inc., provided drafts and editorial assistance to the authors during preparation of this manuscript. D.M. Sullivan is retired. Lastly, the authors would like to posthumously acknowledge Dr. Robert J. Gillies for all his efforts, insights, and support in the development of this project and manuscript. The funding agencies have not played any role in study design, data collection, data analysis, interpretation, writing of the report, and the decision to submit it for publication.

Note

Supplementary data for this article are available at Cancer Research Online (http://cancerres.aacrjournals.org/).

Received March 22, 2024; revised August 19, 2024; accepted October 24, 2024; published first October 30, 2024.

References

1. Moore DC, Oxencis CJ, Shank BR. New and emerging pharmacotherapies for management of multiple myeloma. Am J Health Syst Pharm 2022;79:1137–45.
2. Mimura N, Hideshima T, Anderson KC. Novel therapeutic strategies for multiple myeloma. Exp Hematol 2015;43:732–41.

3. Dimopoulos MA, Jakubowiak AJ, McCarthy PL, Orlowski RZ, Attal M, Bladé J, et al. Developments in continuous therapy and maintenance treatment approaches for patients with newly diagnosed multiple myeloma. Blood Cancer J 2020;10:17.
4. Wallington-Beddoe CT, Mynott RL. Prognostic and predictive biomarker developments in multiple myeloma. J Hematol Oncol 2021;14:151.
5. Kumar SK, Callander NS, Adekola K, Anderson L, Baljevic M, Campagnaro E, et al. Multiple myeloma, version 3.2021, NCCN clinical practice guidelines in oncology. J Natl Compr Canc Netw 2020;18:1685–717.
6. Slatko BE, Gardner AF, Ausubel FM. Overview of next-generation sequencing technologies. Curr Protoc Mol Biol 2018;122:e59.
7. Wang Y, Gali VL, Xu-Monette ZY, Sano D, Thomas SK, Weber DM, et al. Molecular and genetic biomarkers implemented from next-generation sequencing provide treatment insights in clinical practice for Waldenström macroglobulinemia. Neoplasia 2021;23:361–74.
8. Bustoros M, Mouhieddine TH, Detappe A, Ghobrial IM. Established and novel prognostic biomarkers in multiple myeloma. Am Soc Clin Oncol Educ Book 2017;37:548–60.
9. Silva A, Silva MC, Sudalagunta P, Distler A, Jacobson T, Collins A, et al. An ex vivo platform for the prediction of clinical response in multiple myeloma. Cancer Res 2017;77:3336–51.
10. Sudalagunta P, Silva MC, Canevarolo RR, Alugubelli RR, DeAvila G, Tungesvik A, et al. A pharmacodynamic model of clinical synergy in multiple myeloma. EBioMedicine 2020;54:102716.
11. Yadav B, Pemovska T, Szwajda A, Kulesskiy E, Kontro M, Karjalainen R, et al. Quantitative scoring of differential drug sensitivity for individually optimized anticancer therapies. Sci Rep 2014;4:5193.
12. Lin L, Tong Y, Straube J, Zhao J, Gao Y, Bai P, et al. Ex-vivo drug testing predicts chemosensitivity in acute myeloid leukemia. J Leukoc Biol 2020;107:859–70.
13. Touzeau C, Dousset C, Le Gouill S, Sampath D, Leverson JD, Souers AJ, et al. The Bcl-2 specific BH3 mimetic ABT-199: a promising targeted therapy for t(11;14) multiple myeloma. Leukemia 2014;28:210.
14. Kumar SK, Vij R, Kaufman JL, Mikhael JR, Facon T, Pegourie B, et al. Safety and efficacy of venetoclax (ABT-199/GDC-0199) monotherapy for relapsed/refractory multiple myeloma: phase 1 preliminary results. Blood 2015;126:4219.
15. Grosicki S, Simonova M, Spicka I, Pour L, Kriachok I, Gavriatopoulou M, et al. Once-per-week selinexor, bortezomib, and dexamethasone versus twice-per-week bortezomib and dexamethasone in patients with multiple myeloma (BOSTON): a randomised, open-label, phase 3 trial. Lancet 2020;396:1563–73.
16. Gasparetto C, Lipe B, Tuchman S, Callander NS, Lentzsch S, Baljevic M, et al. Once weekly selinexor, carfilzomib, and dexamethasone (SKd) in patients with relapsed/refractory multiple myeloma (MM). J Clin Oncol 2020;38(Suppl 15):8530.
17. Gasparetto C, Lentzsch S, Schiller G, Callander N, Tuchman S, Chen C, et al. Selinexor, daratumumab, and dexamethasone in patients with relapsed or refractory multiple myeloma. EJHaem 2021;2:56–65.
18. Cohen YC, Zada M, Wang S-Y, Bentur OS, Chubar E, Cohen A, et al. Single cell RNA sequencing in patients enrolled in a selinexor clinical trial reveals overexpression of alternative nuclear export pathways associated with resistance to selinexor in refractory multiple myeloma. Blood 2021;138(Suppl 1):2725.
19. Silva A, Jacobson T, Meads M, Distler A, Shain K. An organotypic high throughput system for characterization of drug sensitivity of primary multiple myeloma cells. J Vis Exp 2015;15:e53070.
20. Bishop RT, Miller AK, Froid M, Nerlakanti N, Li T, Frieling JS, et al. The bone ecosystem facilitates multiple myeloma relapse and the evolution of heterogeneous drug resistant disease. Nat Commun 2024;15:2458.
21. van der Maaten L, Hinton G. Visualizing data using t-SNE. J Mach Learn Res 2008;9:2579–605.
22. Bezdek JC, Ehrlich R, Full W. FCM: the fuzzy c-means clustering algorithm. Comput Geosci 1984;10:191–203.
23. Chen EY, Tan CM, Kou Y, Duan Q, Wang Z, Meirelles GV, et al. Enrichr: interactive and collaborative HTML5 gene list enrichment analysis tool. BMC Bioinformatics 2013;14:128.
24. Maura F, Rustad EH, Yellapantula V, Łuksza M, Hoyos D, Maclachlan KH, et al. Role of AID in the temporal pattern of acquisition of driver mutations in multiple myeloma. Leukemia 2020;34:1476–80.
25. Leblay N, Ahn S, Tilmont R, Poorebrahim M, Maity R, Lee H, et al. Integrated epigenetic and transcriptional single-cell analysis of t(11;14) multiple myeloma and its BCL2 dependency. Blood 2024;143:42–56.
26. Punnoose EA, Leverson JD, Peale F, Boghaert ER, Belmont LD, Tan N, et al. Expression profile of BCL-2, BCL-XL, and MCL-1 predicts pharmacological response to the BCL-2 selective antagonist venetoclax in multiple myeloma models. Mol Cancer Ther 2016;15:1132–44.
27. Neri P, Barwick BG, Jung D, Patton JC, Maity R, Tagoug I, et al. ETV4-Dependent transcriptional plasticity maintains MYC expression and results in IMiD resistance in multiple myeloma. Blood Cancer Discov 2024;5:56–73.
28. Slomp A, Moesbergen LM, Gong J-N, Cuenca M, von dem Borne PA, Sonneveld P, et al. Multiple myeloma with 1q21 amplification is highly sensitive to MCL-1 targeting. Blood Adv 2019;3:4202–14.
29. An G, Xu Y, Shi L, Zou D, Deng S, Sui W, et al. t(11;14) multiple myeloma: a subtype associated with distinct immunological features, immunophenotypic characteristics but divergent outcome. Leuk Res 2013;37:1251–7.
30. Mithraprabhu S, Khong T, Spencer A. Overcoming inherent resistance to histone deacetylase inhibitors in multiple myeloma cells by targeting pathways integral to the actin cytoskeleton. Cell Death Dis 2014;5:e1134.
31. Desai S, Maurin M, Smith MA, Bolick SCE, Dessureault S, Tao J, et al. PRDM1 is required for mantle cell lymphoma response to bortezomib. Mol Cancer Res 2010;8:907–18.
32. Zhou F, Zhou N. CYLD in hematological malignancies. Ann Case Rep 2021;6:606.
33. Subramanian A, Kuehn H, Gould J, Tamayo P, Mesirov JP. GSEA-P: a desktop application for gene set enrichment analysis. Bioinformatics 2007;23:3251–3.
34. Liberzon A, Birger C, Thorvaldsdóttir H, Ghandi M, Mesirov JP, Tamayo P. The Molecular Signatures Database (MSigDB) hallmark gene set collection. Cell Syst 2015;1:417–25.
35. Ogata H, Goto S, Fujibuchi W, Kanehisa M. Computation with the KEGG pathway database. Biosystems 1998;47:119–28.
36. Zhan F, Huang Y, Colla S, Stewart JP, Hanamura I, Gupta S, et al. The molecular classification of multiple myeloma. Blood 2006;108:2020–8.
37. Shain KH, Yarde DN, Meads MB, Huang M, Jove R, Hazlehurst LA, et al. Beta1 integrin adhesion enhances IL-6-mediated STAT3 signaling in myeloma cells: implications for microenvironment influence on tumor survival and proliferation. Cancer Res 2009;69:1009–15.
38. Meads MB, Gatenby RA, Dalton WS. Environment-mediated drug resistance: a major contributor to minimal residual disease. Nat Rev Cancer 2009;9:665–74.
39. Hazlehurst LA, Enkemann SA, Beam CA, Argilagos RF, Painter J, Shain KH, et al. Genotypic and phenotypic comparisons of de novo and acquired melphalan resistance in an isogenic multiple myeloma cell line model. Cancer Res 2003;63:7900–6.
40. Goel S, DeCristo MJ, Watt AC, BrinJones H, Sceneay J, Li BB, et al. CDK4/6 inhibition triggers anti-tumour immunity. Nature 2017;548:471–5.
41. Skerget S, Penaherrera D, Chari A, Jagannath S, Siegel DS, Vij R, et al. Comprehensive molecular profiling of multiple myeloma identifies refined copy number and expression subtypes. Nat Genet 2024;56:1878–89.
42. Gooding S, Ansari-Pour N, Kazeroun M, Karagoz K, Polonskaia A, Salazar M, et al. Loss of COP9 signalosome genes at 2q37 is associated with IMiD resistance in multiple myeloma. Blood 2022;140:1816–21.
43. Trasanidis N, Katsarou A, Ponnusamy K, Shen Y-A, Kostopoulos IV, Bergonia B, et al. Systems medicine dissection of chr1q-amp reveals a novel PBX1-FOXM1 axis for targeted therapy in multiple myeloma. Blood 2022;139:1939–53.
44. Dibb M, Han N, Choudhury J, Hayes S, Valentine H, West C, et al. The FOXM1-PLK1 axis is commonly upregulated in oesophageal adenocarcinoma. Br J Cancer 2012;107:1766–75.
45. Fu Z, Malureanu L, Huang J, Wang W, Li H, van Deursen JM, et al. Plk1-dependent phosphorylation of FoxM1 regulates a transcriptional programme required for mitotic progression. Nat Cell Biol 2008;10:1076–82.
46. Chen L, Yap JL, Yoshioka M, Lanning ME, Fountain RN, Raje M, et al. BRD4 structure-activity relationships of dual PLK1 kinase/BRD4 bromodomain inhibitor BI-2536. ACS Med Chem Lett 2015;6:764–9.
47. Markovina S, Callander NS, O'Connor SL, Kim J, Werndli JE, Raschko M, et al. Bortezomib-resistant nuclear factor-kappaB activity in multiple myeloma cells. Mol Cancer Res 2008;6:1356–64.
48. Duvefelt CF, Lub S, Agarwal P, Arngården L, Hammarberg A, Maes K, et al. Increased resistance to proteasome inhibitors in multiple myeloma mediated

by cIAP2—implications for a combinatorial treatment. Oncotarget 2015;6: 20621–35.
49. Cai Y, Li B, Peng D, Wang X, Li P, Huang M, et al. Crm1-dependent nuclear export of Bach1 is involved in the protective effect of hyperoside on oxidative damage in hepatocytes and CCl_4-induced acute liver injury. J Inflamm Res 2021;14:551–65.
50. Igarashi K, Nishizawa H, Saiki Y, Matsumoto M. The transcription factor BACH1 at the crossroads of cancer biology: from epithelial–mesenchymal transition to ferroptosis. J Biol Chem 2021;297:101032.
51. Yu W, Cui X, Wan Z, Yu Y, Liu X, Jin L. Silencing forkhead box M1 promotes apoptosis and autophagy through SIRT7/mTOR/IGF2 pathway in gastric cancer cells. J Cell Biochem 2018;119:9090–8.
52. Lin J-Z, Wang W-W, Hu T-T, Zhu G-Y, Li L-N, Zhang C-Y, et al. FOXM1 contributes to docetaxel resistance in castration-resistant prostate cancer by inducing AMPK/mTOR-mediated autophagy. Cancer Lett 2020;469: 481–9.
53. Lee N-R, Kim D-Y, Jin H, Meng R, Chae OH, Kim S-H, et al. Inactivation of the Akt/FOXM1 signaling pathway by panobinostat suppresses the proliferation and metastasis of gastric cancer cells. Int J Mol Sci 2021;22:5955.
54. Zhang N, Wei P, Gong A, Chiu W-T, Lee H-T, Colman H, et al. FoxM1 promotes β-catenin nuclear localization and controls wnt target-gene expression and glioma tumorigenesis. Cancer Cell 2011;20:427–42.
55. Xu F, Zhu Y, Lu Y, Yu Z, Zhong J, Li Y, et al. Anthelmintic pyrvinium pamoate blocks Wnt/β-catenin and induces apoptosis in multiple myeloma cells. Oncol Lett 2018;15:5871–8.
56. Gomes AR, Zhao F, Lam EWF. Role and regulation of the forkhead transcription factors FOXO3a and FOXM1 in carcinogenesis and drug resistance. Chin J Cancer 2013;32:365–70.
57. Zhang C, Zhang J, Wang G, Xu J, Li Y, Guo Q, et al. Benefit of Sunitinib in the treatment of pulmonary primitive neuroectodermal tumors: a case report and literature review. Oncotarget 2016;7:87543–51.
58. Halasi M, Gartel AL. Suppression of FOXM1 sensitizes human cancer cells to cell death induced by DNA-damage. PLoS One 2012;7:e31761.
59. Chesnokov MS, Borhani S, Halasi M, Arbieva Z, Khan I, Gartel AL. FOXM1-AKT positive regulation loop provides venetoclax resistance in AML. Front Oncol 2021;11:696532.
60. Webb BM, Bryson BL, Williams-Medina E, Bobbitt JR, Seachrist DD, Anstine LJ, et al. TGF-β/activin signaling promotes CDK7 inhibitor resistance in triple-negative breast cancer cells through upregulation of multidrug transporters. J Biol Chem 2021;297:101162.
61. Song S, Zhang R, Cao W, Fang G, Yu Y, Wan Y, et al. Foxm1 is a critical driver of TGF-β-induced EndMT in endothelial cells through Smad2/3 and binds to the Snail promoter. J Cell Physiol 2019;234:9052–64.
62. Gu C, Jing X, Holman C, Sompallae R, Zhan F, Tricot G, et al. Upregulation of FOXM1 leads to diminished drug sensitivity in myeloma. BMC Cancer 2018;18: 1152.
63. Amatangelo M, Ortiz M, Neri P, Towfic F, Bjorklund C, Kang J, et al. FOXM1 is associated with development of therapeutic resistance in multiple myeloma. Blood 2017;130(Suppl 1):1261.
64. Li J, Ohmura S, Marchetto A, Orth MF, Imle R, Dallmayer M, et al. Therapeutic targeting of the PLK1-PRC1-axis triggers cell death in genomically silent childhood cancer. Nat Commun 2021;12:5356.
65. Mancini M, De Santis S, Monaldi C, Bavaro L, Martelli M, Castagnetti F, et al. Hyper-activation of Aurora kinase a-polo-like kinase 1-FOXM1 axis promotes chronic myeloid leukemia resistance to tyrosine kinase inhibitors. J Exp Clin Cancer Res 2019;38:216.
66. Palumbo A, Chanan-Khan A, Weisel K, Nooka AK, Masszi T, Beksac M, et al. Daratumumab, bortezomib, and dexamethasone for multiple myeloma. N Engl J Med 2016;375:754–66.
67. Tatarova Z, Blumberg DC, Korkola JE, Heiser LM, Muschler JL, Schedin PJ, et al. A multiplex implantable microdevice assay identifies synergistic combinations of cancer immunotherapies and conventional drugs. Nat Biotechnol 2022;40:1823–33.
68. Qi W, Zhang W, Edwards H, Chu R, Madlambayan GJ, Taub JW, et al. Synergistic anti-leukemic interactions between panobinostat and MK-1775 in acute myeloid leukemia ex vivo. Cancer Biol Ther 2015;16:1784–93.
69. Mukherjee N, Amato CM, Skees J, Todd KJ, Lambert KA, Robinson WA, et al. Simultaneously inhibiting BCL2 and MCL1 is a therapeutic option for patients with advanced melanoma. Cancers (Basel) 2020;12:2182.
70. Harrison S, Cavo M, De La Rubia J, Popat R, Gasparetto C, Hungria VT, et al. T(11;14) and high BCL2 expression are predictive biomarkers of response to venetoclax in combination with bortezomib and dexamethasone in patients with relapsed/refractory multiple myeloma: biomarker analyses from the phase 3 Bellini study. Blood 2019;134(Suppl 1):142.
71. Gatenby RA, Brown J, Vincent T. Lessons from applied ecology: cancer control using an evolutionary double bind. Cancer Res 2009;69:7499–502.
72. Lawrence MS, Stojanov P, Polak P, Kryukov GV, Cibulskis K, Sivachenko A, et al. Mutational heterogeneity in cancer and the search for new cancer-associated genes. Nature 2013;499:214–18.
73. Wong CH, Siah KW, Lo AW. Estimation of clinical trial success rates and related parameters. Biostatistics 2019;20:273–86.